1970

Electric field strength dependency of the rate of radiation induced degradation in silicon planar devices

Cyrus Hoshang Irani

Department:

ELECTRIC FIELD STRENGTH DEPENDENCY OF THE RATE OF RADIATION INDUCED DEGRADATION IN SILICON PLANAR DEVICES

BY

CYRUS HOSHANG IRANI, 1945-

A

THESIS

submitted to the faculty of

UNIVERSITY OF MISSOURI-ROLLA

in partial fulfillment of the requirements for the

Degree of

MASTER OF SCIENCE IN NUCLEAR ENGINEERING

Rolla, Missouri

1970

Approved by

Charles A. Goben
(Advisor)

Albert E. Bolon

Fred C. Blanchard

ABSTRACT

The investigation of electric field strength dependence of the rate of damage introduction, caused by gamma and neutron irradiations in matched silicon planar epitaxial transistors is reported. Groups of devices (with varying biases applied to the emitter-base and collector-base junctions to allow study of the electric field strength dependence) were exposed to ionizing gamma radiation from a Co-60 source. Similar experiments were conducted to study the field strength dependence of the rate of space-charge volume damage introduction, caused by fast neutrons (E>10keV, fission source).

The experimental results indicate that the rate of surface degradation, as reflected by the increase of the normalized surface base current component ($\Delta I_B(\gamma)/I_B(0)$) and the reciprocal of the surface minority carrier lifetime is an increasing function of the electric field strength and the total gamma dose ($1x10^4$ rads (Si) $< \gamma <$ $1x10^6$ rads (Si)). The ionizing gamma induced surface effects are significant at low fluences in the swimming pool type reactor and have to be subtracted from the total variation in transistor parameters (junction capacitance and base current component) before a meaningful interpretation of the fast neutron induced bulk effects can be given. The rate of volume damage introduction, K_v, was investigated in an effort to explain the anamalous behavior of fast neutron induced defect clusters in the high field space charge region of silicon p-n junctions. K_v is observed to be an increasing function of the average electric field strength in the p-n junction during irradiation and a decreasing function of the neutron fluence. Empirical expressions for the surface degradation and rate of volume damage introduction are developed.

TABLE OF CONTENTS

Page

LIST OF ILLUSTRATIONS

LIST OF TABLES

LIST OF APPENDICES

LIST OF ILLUSTRATIONS FOR APPENDICES

I. INTRODUCTION

Extensive experimental and theoretical investigations[1-16] have established the principal characteristics of radiation-induced parameter changes in transistors. The parameter changes of major importance studied are the increase in the base current component (ΔI_B), the increase in the reciprocal common-emitter current gain $\left[\Delta(1/h_{FE})\right]$, the increase in the reciprocal minority carrier lifetime $\left[\Delta(1/\tau)\right]$, and the change in junction capacitance $\left[\Delta C\right]$. These parameter changes are a direct result of ionizing radiation induced surface damage, fast neutron induced displacement damage in the bulk space-charge and bulk neutral region, or a combination of the two. Many previous studies[1-11] of radiation damage effects on transistor properties have been conducted with the transistor junctions passive during irradiation. For transistor applications in circuits, the devices are usually active (i.e., bias applied at one or both junctions) during irradiation. It is necessary, therefore, to investigate the effect of biasing the junctions during irradiation to obtain a correlation between the electric field strength in the junction during irradiation and the parameter changes of interest.

In analyzing nuclear radiation damage, it is frequently necessary to calculate the effect of a mixed spectrum of neutrons and ionizing gamma radiation. Such a situation is encountered in research type reactors, such as the University of Missouri - Rolla, 200 kW, BSR type Swimming pool reactor (See Appendix D). The ionizing radiation produced from the fission products in the reactor core is often of considerable magnitude and is a dominant cause of transistor gain degradation at low neutron fluences. The ionizing radiation induced surface current

components and junction capacitance increase must be subtracted from the total observed changes before displacement damage effects can be meaningfully analyzed. The first part of this research effort is concerned with ionizing radiation induced surface effects, produced from a Co-60 pure gamma source. The second part of the investigation analyzes the fast neutron damage in the bulk space charge region of a p-n junction after surface effects have been subtracted. Previous investigations have established that the response of silicon planar transistors to ionizing radiation varies with the initial conditions[1-3] at the Si-SiO_2 interface and the junction bias applied during irradiation[4-7]. The degradation in silicon surface properties is manifested by the enhancement, depletion or inversion of silicon surfaces caused by the accumulation of space-charge in the SiO_2 layer above the Si surface resulting in changes in the surface potential of the semiconductor. Further, the accumulation of surface states alters the surface recombination velocity of minority carriers in the p-n junction[4,5,7]. The field dependencies of the gamma induced parameter changes investigated here are the decrease in the reciprocal forward current gain (as reflected by the increase in the gamma induced surface base current component), the surface recombination velocity (as reflected by the increase in the reciprocal of the minority carrier lifetime) and the junction capacitance. The devices used were specially fabricated matched silicon planar epitaxial transistors, whose emitter-base and collector-base junctions were biased to different voltages during gamma irradiation to study the field strength dependency.

Neutron induced defect clusters in silicon transistors have been shown[8-13] to behave differently in the high field emitter-base "space-charge" region than in the low field "neutral" bulk base region, both during introduction and annealing. This anomalous behavior in both formation and annealing has been attributed by some authors to carrier density effects[14] or to a modification of the defect cluster by the presence of an electric field[12,13]. It was therefore thought necessary to determine if such a field dependence existed through a study of the variation of the rate of space-charge volume damage introduction, K_v, with junction electric field strength. Goben[11] has shown that the neutron induced base current component of base current originates in the bulk space-charge region of the emitter-base junction. Hence, it should be dependent on the volume of that region. Su et al.[12,15], assumed that K_v was a constant at all values of neutron fluence. However, since K_1 is volume independent and a constant for all ranges of neutron fluence[15,16], one would expect K_v to decrease with increasing neutron fluence, since $K_v = K_1/x_m$, where x_m is the depletion layer width at a particular bias voltage and can be obtained from capacitance-voltage measurements from $x_m = A_E \cdot \epsilon\epsilon_o/C$. Groups of matched silicon planar expitaxial devices, with various biases applied to the emitter-base junction, were irradiated to various neutron fluences to study the electric field strength and neutron fluence dependencies of K_v. The gamma induced parameter changes had to be subtracted before meaningful values of K_v could be obtained.

II. ELECTRIC FIELD STRENGTH DEPENDENCE OF THE IONIZING RADIATION INDUCED SURFACE DAMAGE

A. Introduction

Experimental and theoretical investigations[1-7, 17-19] have established that the response of silicon planar transistors to ionizing radiation varies with the initial conditions at the Si-SiO_2 interface and the junction bias applied during irradiation. The degradation in silicon surface properties is manifested by the enhancement, depletion or inversion of silicon surfaces caused by the accumulation of space charge in the SiO_2 layer above the Si surface resulting in changes in the surface potential of the semiconductor and, further, the accumulation of surface states alters the surface recombination velocity in the p-n junction. The field strength dependencies of the gamma induced parameter changes investigated here are the increase in the reciprocal forward current gain (as reflected by the increase in the gamma induced base current component), the increase in the surface recombination velocity (increase in the reciprocal of the minority carrier lifetime) and the junction capacitance.

B. Experimental Procedure

The devices used in the present investigation were specially fabricated silicon planar epitaxial matched transistors (SA7472) manufactured by Texas Instruments. Groups of devices with varying biases applied to the emitter-base and collector-base junctions (to study the electric field strength dependence) were exposed to ionizing gamma radiation. The gamma radiation was obtained from a 5000 Curie Cobalt-60 source, at the University of Missouri - Columbia Research Reactor Facility.

Current-voltage characteristics for the test devices before and after each irradiation step were measured and recorded by an Automatic Data Acquisition System[20,21], with an overall absolute accuracy of $\pm 1\%$ of reading and a precision of $\pm 0.3\%$ of reading in the range from 10^{-10} amperes to 2×10^{-1} amperes (over 9 decades). For comparison of devices with various geometries, the perimeter dependence of the base-emitter region[22] was normalized by dividing by the pre-irradiation base current, I_{BO}. The Tektronix oscilloscope[23] Type 555 with the Tektronix Type S Recovery-time plug-in Unit was used for lifetime measurements. The effective minority carrier lifetime is the time necessary for the number of minority carriers injected during forward conduction of a p-n junction to decrease to 0.367 (1/e) of the original number after termination of the forward currents. The junction capacitance was measured by a Micro-Instrument Digital Capacitance Tester[24] and corrected for socket and header capacitances. Current-voltage characteristics, junction capacitance and lifetime measurements were measured at room temperature (27°C) after each irradiation step.

C. Field Strength Dependence of the Gamma-Induced Surface Current Components

The reduction in transistor current gain by ionizing radiation-induced surface effects is caused by introduction of additional base current components[25]. The two base current components generated by ionizing radiation, which dominate ($1/h_{FE}$) at low currents are surface recombination-generation current, I_{SRG}, and surface channel current, I_{CH}[25]. The I_{SRG} component is produced by recombination in the base-emitter space-charge region at the SiO_2-Si interface where a high concentration of recombination centers exists. The I_{SRG} current

component varies with base-emitter forward voltage as exp (qV_{BE}/nkT), where the typical[25] range of n is 1.3 to 2. The surface channel component of current I_{CH}, at the base-emitter junction also varies as exp (qV_{BE}/nkT). The exponential slope term, n, for this case, is greater than 2.

Figure II-1 is a plot of the current-voltage characteristics of test device #21 (emitter-base junction reverse biased to 3.0 volts during irradiation) from pre-irradiation to saturation dose levels. At lower current levels, the reciprocal slope term "n" is seen to increase from 1.4 before irradiation to 2.25 at a saturation dose level of $\approx 10^6$ rads (Si). This indicates that the I_{SRG} current component dominates at lower doses, and the I_{CH} current component dominates at doses near saturation and that the channel is very small. This would be expected since the build up of space charge in the oxide increases with the accumulated dose until it is of sufficient magnitude to invert the p type base at the surface, (heavily doped on the emitter side) resulting in channel formation. Interestingly, "n" is observed to be a constant over a wide range of current levels at low and moderate current levels. At higher current levels "n" is observed to decrease slightly as would be expected from increased recombination in the bulk base region at higher levels. To study the surface degradation at the collector-base junction, current-voltage characteristics were taken with the device operating in the inverse configuration. Figure II-2 is a plot of the I-V characteristics of device #23 (collector-base junction reverse biased to 3.0 volts during irradiation) at different doses. The reciprocal slope term, "n", is observed to increase very rapidly from 1.23 before irradiation to 7.4 at saturation doses. Similar values

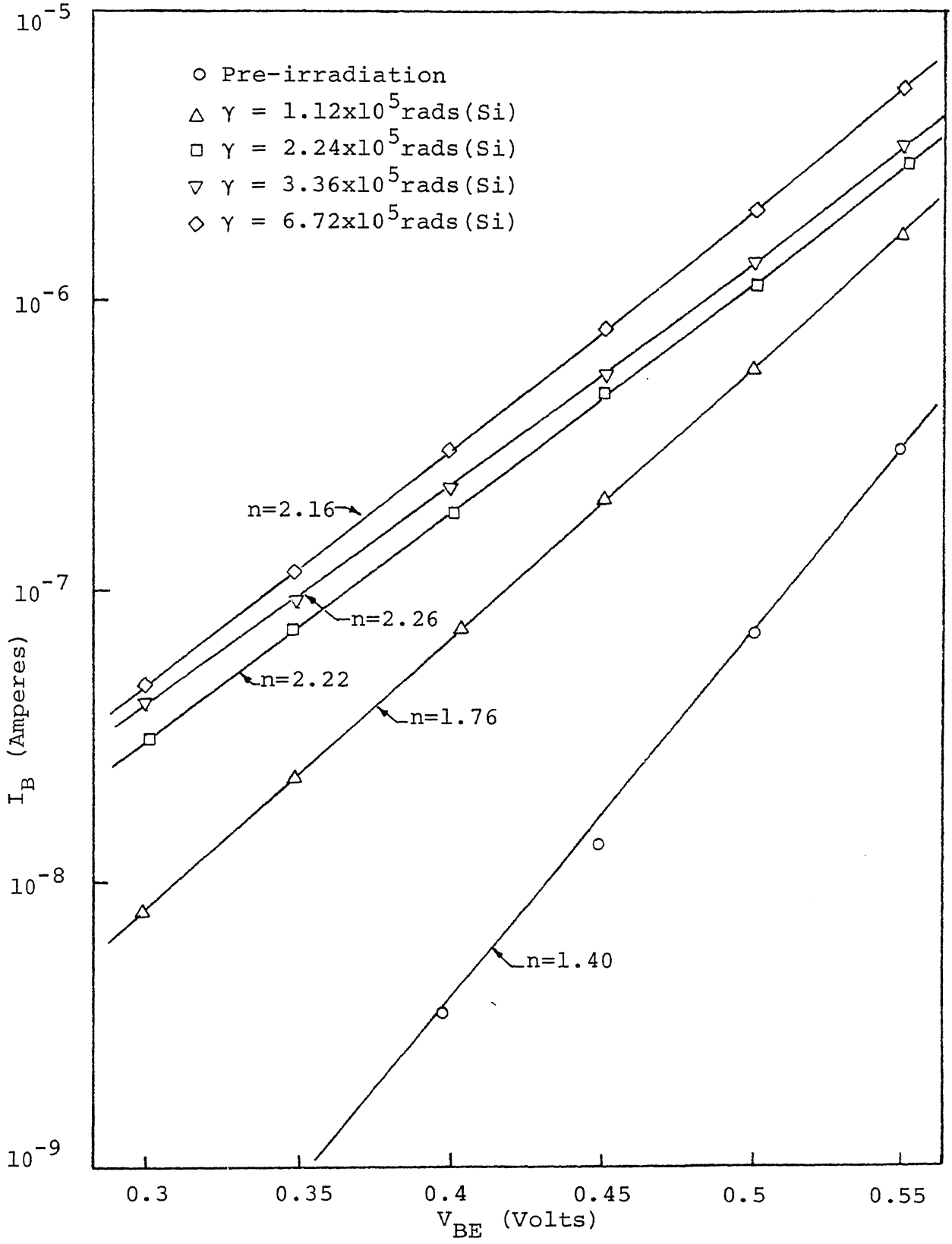

Figure II-1. Current versus voltage for device # 21 at different dose levels with the emitter-base junction reverse biased to 3.0 volts during irradiation.

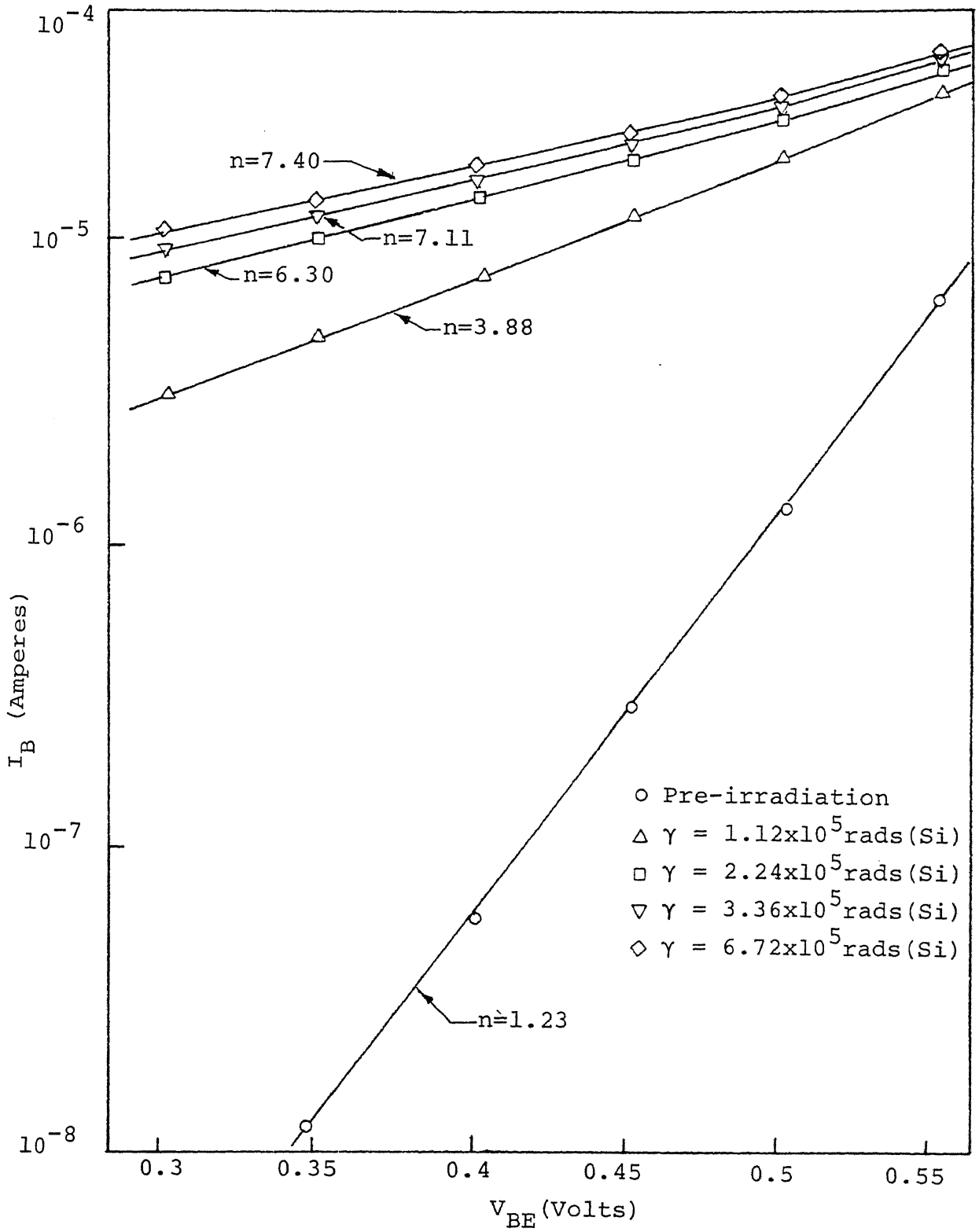

Figure II-2. Current versus voltage for device # 23 at different dose levels with the collector-base junction reverse biased to 3.0 volts during irradiation.

for the reciprocal slope term, "n", were obtained by Sah[25] indicating the dominance of the surface channel current component. The observed channel formation at low gamma doses on the collector side of the p-type base can be attributed to a lower dopant concentration at the surface (caused by diffusion of impurity atoms under the oxide mask during fabrication) resulting in inversion at much lower doses.

Table II-1 lists the normalized increase in base current for gamma doses from 1.12×10^5 to 1.34×10^6 rads (Si) for the three bias conditions at the emitter-base junction during irradiation. The base currents were measured at V_{BE} = 500mV, $I_C = 5\mu A$.

TABLE II-1. Normalized base current increase for SA7472 devices (#21, #27, #08) at different gamma doses.

Total Gamma Dose Rads (Si)	Device #21 E=1.26×10^5 V/cm $\frac{\Delta I_B(\gamma)}{I_B(o)}$	Device #27 E=4.6×10^4 V/cm $\frac{\Delta I_B(\gamma)}{I_B(o)}$	Device #08 E=2.71×10^4 V/cm $\frac{\Delta I_B(\gamma)}{I_B(o)}$
1.12×10^5	7.5	3.5	2.6
2.24×10^5	15.5	7.9	7.2
3.36×10^5	18.2	11.5	9.1
6.72×10^5	23.0	16.9	12.5
1.01×10^6	25.5	18.4	13.9
1.34×10^6	25.2	17.2	15.0

The changes with gamma irradiation are seen more readily if one plots the change in base current, normalized by the pre-irradiation base current versus the total absorbed gamma dose. Figure II-3 illustrates a group of such plots (Curves A, B, C) from the data in Table II-1 for the three field strengths used in this study. The form of the curves may be immediately recognized from this plot as $K\{1-\exp(-\alpha\gamma)\}$ and in particular, one may write:

$$\frac{\Delta I_B(V_{BE}, E_r, \gamma)}{I_{BO}(V_{BE})} = K_s(E_r) \cdot \{1-\exp(-\alpha(E_r) \cdot \gamma)\} \quad \text{(II-1)}$$

where the damage saturation parameter, K_s, and damage introduction rate, α, are called out explicitly as functions of the junction electric field strength present during exposure (E_r). Plotting K_s versus the average junction electric field strength gives the expressions:

$$K_s(E_r) = 0.19 \times E_r^{0.42} \quad \text{(II-2)}$$

Similarly $\alpha(E_r)$ may be written as:

$$\alpha(E_r) = 1.67 \times 10^{-6} + E_r(1.40 \times 10^{-11})$$

$$= (1 + E_r/1.2 \times 10^5)/6.0 \times 10^5 \quad \text{(II-3)}$$

Combining equations (II-1), (II-2) and (II-3) yields the empirical equation:

$$\Delta I_B(V_{BE}, E_r, \gamma) \Big/ I_{BO}(V_{BE}) = 0.19E_r^{0.42}$$

$$\cdot\{1-\exp[(1 + E/1.2 \times 10^5) \cdot \gamma/6.0 \times 10^5]\} \quad \text{(II-4)}$$

The solid lines (A, B, C) in Figure II-3 are plots of equation (II-4) and good agreement with experimental data are noted. Curves D and E (Figure II-3) are

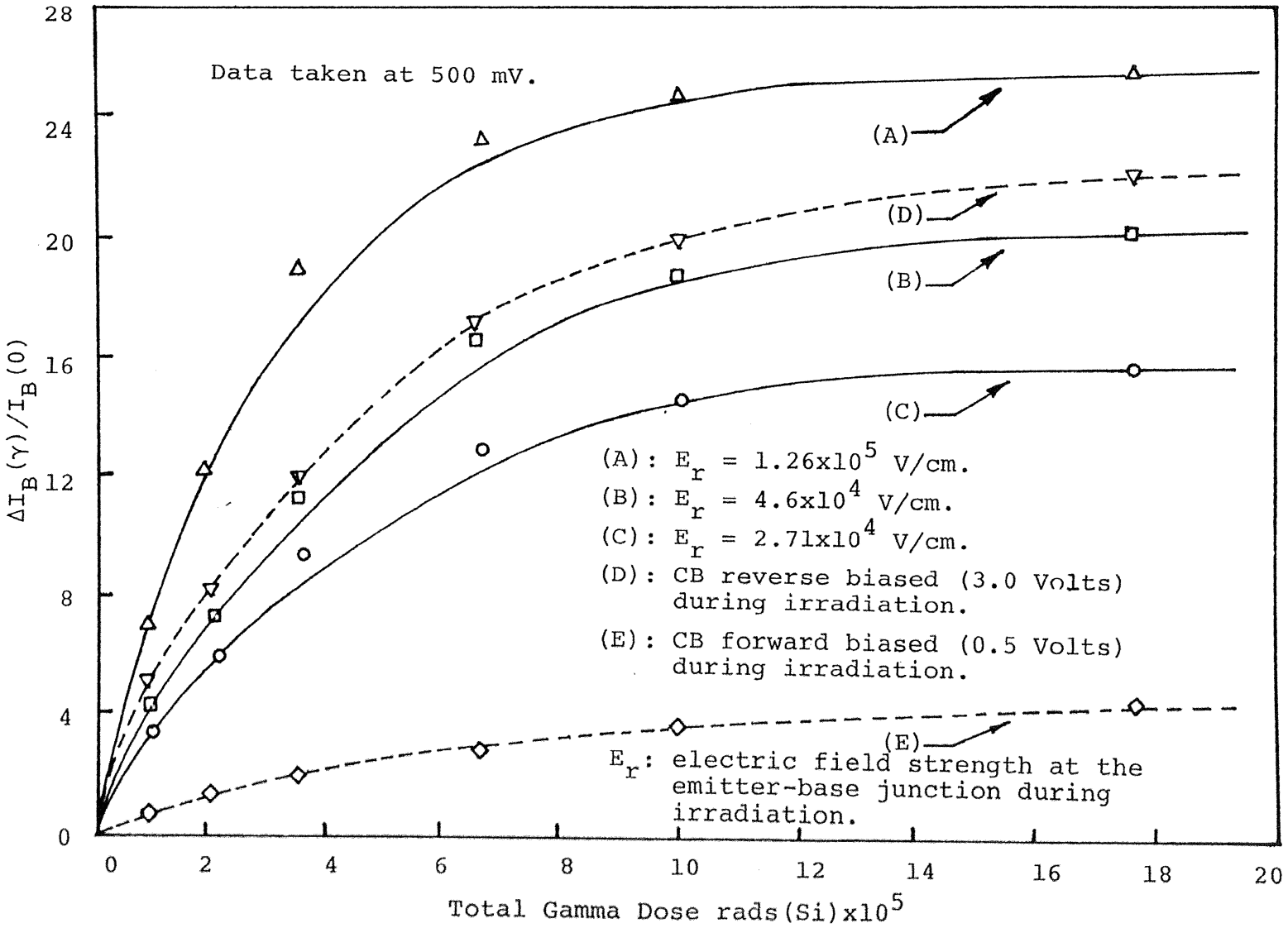

Figure II-3. Normalized base current increase versus total gamma dose for devices with varying junction electric field strengths during irradiation.

typical plots of the normalized increase in the base current versus gamma dose for similar devices with the collector-base junction biased to 3.0 volts (reverse) and 0.5 volts (forward), respectively. The saturation value of the surface damage at the emitter-base junction at larger doses is found to be greater for the reverse biased collector-base junction (Curve D) than for both junctions unbiased (Curve B) and the forward biased collector-base junction (Curve E). Similar results have been reported by Nelson and Sweet[5], although no explanation was given by them for the effect of collector-base biasing on the degradation of the emitter efficiency. These results may be explained if one realizes that a reverse biased collector-base junction has the effect of reverse biasing the emitter-base junction, and a forward biased collector-base junction has the effect of forward biasing the emitter-base junction to maintain zero emitter current at the open emitter. For both cases of biasing, surface effects are observed to saturate at about 10^6 rads(Si), as reflected by the very small change in gamma-induced current above this dose.

D. Surface Minority Carrier Lifetime Measurements

Ionizing radiation is known to induce surface states, which act as recombination centers for minority carriers[4,25,26]. The minority-carrier lifetime (related to the reciprocal of the surface recombination velocity) is one of the several parameters used to determine surface degradation of a device. The effect of the junction electric field strength on the degradation of the minority carrier lifetime is investigated by plotting $(1/\tau_B - 1/\tau_0)$ versus the accumulated gamma dose, γ. (τ_0 and τ_B are the pre-irradiation and post-irradiation minority carrier lifetimes, respectively). A typical plot for the special devices is shown in Figure II-4. The form of the curves can be written as:

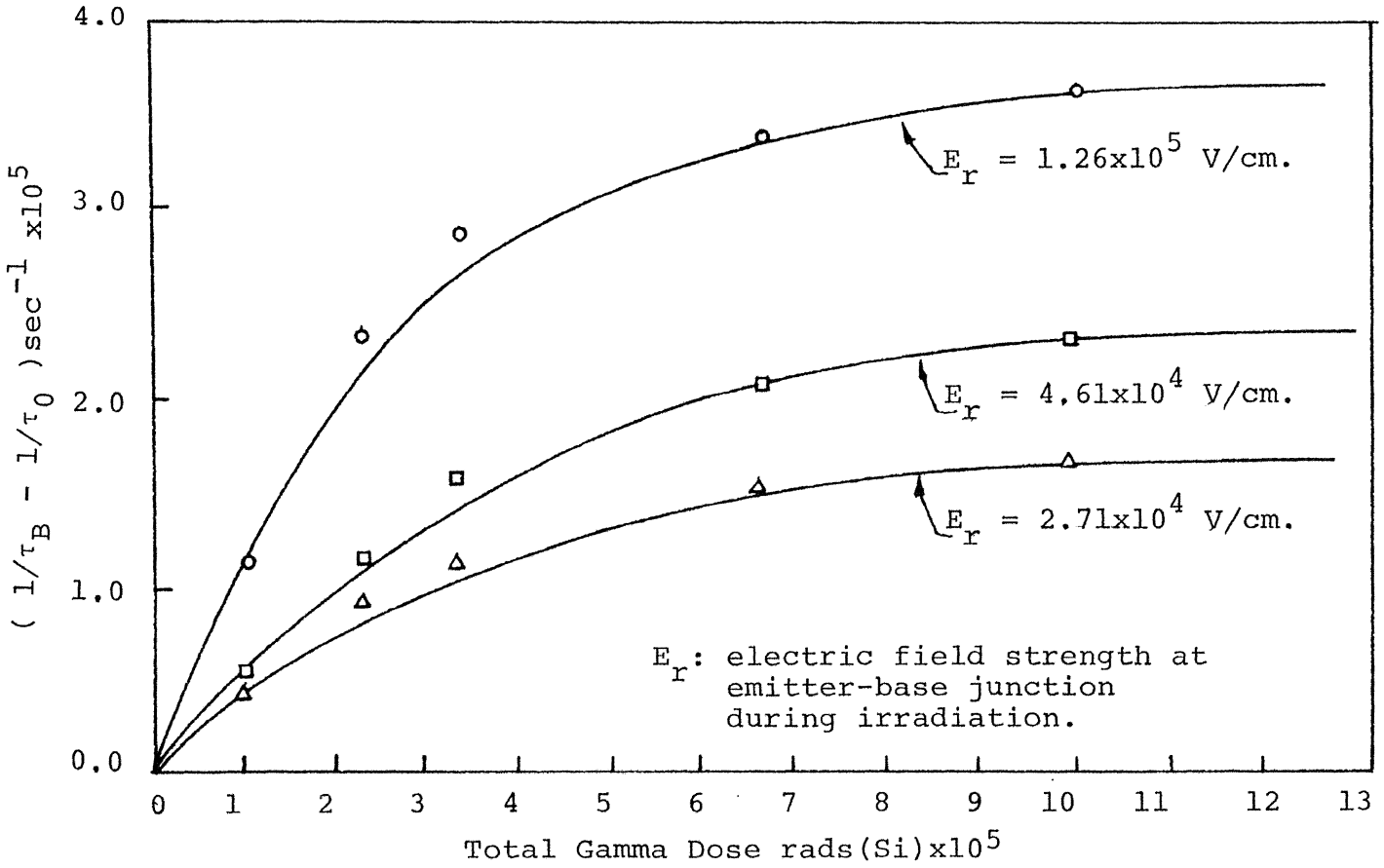

Figure II-4. Change in surface recombination velocity (reciprocal of minority carrier lifetime), versus total gamma dose for devices with varying junction electric field strengths at the emitter-base junction during irradiation.

$$(1/\tau_B - 1/\tau_0) = K_\tau (E_r) \cdot \{1 - \exp(\alpha_\tau (E_r) \cdot \gamma)\} \qquad (\text{II-5})$$

The lifetime saturation parameter, K_τ, can be expressed as:

$$K_\tau (E_r) = K_{\tau 0} \cdot E_r^m = 95.5 \cdot E_r^{0.68} \qquad (\text{II-6})$$

and the lifetime damage introduction rate is given by:

$$\alpha_\tau = (1 + E_r/E_o)/\gamma_0 = (1 + E_r/9.5 \times 10^5)/1.5 \times 10^5 \qquad (\text{II-7})$$

The similarity of the forms of equations (II-1) and (II-5) indicates that the degradation of the surface minority carrier lifetime follows a trend similar to the normalized base current increase. This should be expected since surface states act as recombination centers for the minority carriers, thus increasing both the surface recombination-generation base current component and the surface recombination velocity. It is thus found feasible to use this prediction technique to study changes in junction parameters of silicon planar matched devices having similar initial characteristics (h_{FE}, I_B, τ_B) and operating under different bias conditions when exposed to various doses of ionizing radiation[26].

E. Junction Capacitance-Voltage Measurements

In 1968 Su et al.[7,11], examined the effect of biasing the collector-base junction to various biases during neutron irradiation (in a Swimming Pool Type Reactor Core). The reverse biased device showed a marked increase in capacitance compared to the unbiased and forward biased devices. The increase in capacitance was seen to saturate at a neutron fluence of about 1×10^{14} neutrons/cm^2 indicating that formation of surface channels saturate at a dose of about 10^6 rads (Si) of ionizing radiation which accompanies this neutron fluence. In this study junction

capacitance measurements were made on a group of SA7472 devices at various gamma dose levels. Table II-2 lists the normalized collector-base junction capacitances ($C(\gamma)/C(0)$) for devices with varying electric fields at the collector-base junction during irradiation from 0 to 1.01×10^6 rads (Si):

TABLE II-2. Normalized collector-base junction capacitance for SA7472 devices (#23, #27, #19) at different gamma doses.

Total Gamma Dose Rads (Si)	Device #23 $E=4.9\times10^4$V/cm $\frac{C(\gamma)}{C(0)}$	Device #27 $E=6.33\times10^3$Vcm $\frac{C(\gamma)}{C(0)}$	Device #19 $E=1.20\times10^3$V/cm $\frac{C(\gamma)}{C(0)}$
0.0	1.00	1.00	1.00
1.12×10^5	1.09	0.99	1.00
2.24×10^5	1.08	1.00	1.00
3.36×10^5	1.74	1.02	1.00
6.72×10^5	2.22	1.03	1.01
1.01×10^6	2.22	1.04	1.01

The rapid increase in the junction capacitance for the reverse biased collector-base junction ($E_r = 4.9 \times 10^4$ V/cm) (Figure II-5) indicates an increase in the junction area caused by the formation of surface channels. The resultant I_{CH} current component varies with base collector voltage (the devices were operating in the inverse configuration) as $\exp(qV_{BE}/nkT)$, where n is observed to range from 4 to 7.

The rate of surface degradation, as reflected by the increase in the surface base current component surface recombination velocity and junction capacitance is

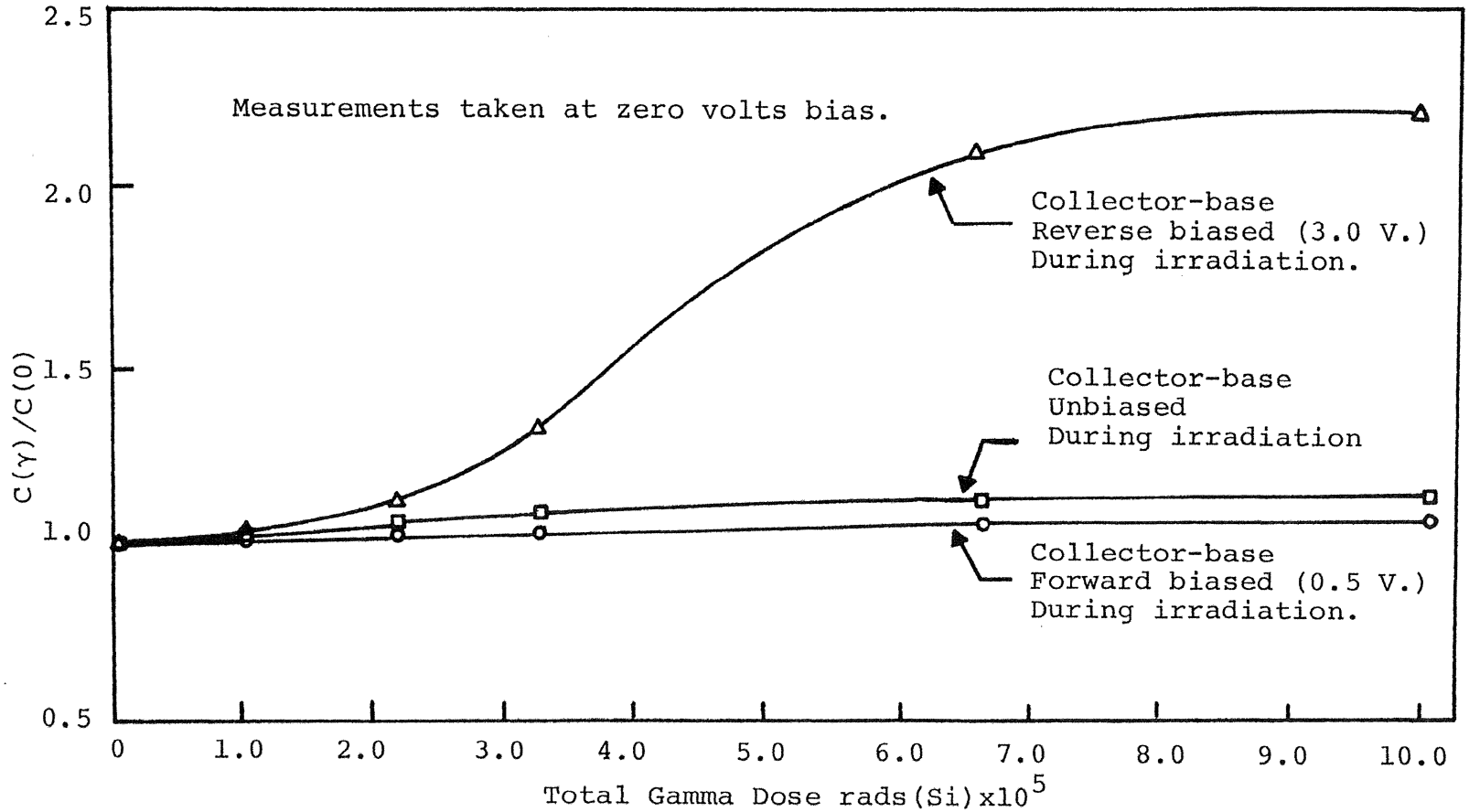

Figure II-5. Normalized collector-base junction capacitance versus total gamma dose for different bias conditions at the collector-base junction during irradiation.

observed to be strongly dependent on the electric field strength at the junction during exposure[26]. This can be attributed to the dependence of the build up of positive charge in the SiO_2 layer above the space-charge region and surface states at the Si-SiO_2 interface on the strength of the junction fringing field. A reverse biased junction, has the maximum fringing electric field strength, and hence one would expect the positive charge build up above the p-type base in the n-p-n device to be the greatest in this case.

III. DETERMINATION OF TRANSISTOR PARAMETER CHANGES CAUSED BY A MIXED FIELD OF NEUTRON AND GAMMA IRRADIATIONS

A. Mechanisms of Interactions of Nuclear Radiation with Semiconductor Materials

As discussed by Larin[27], the observed changes in the electrical behavior of semiconductor devices exposed to a radiation environment are caused by two fundamental effects of radiation in semiconductor material, displacements and ionization. Displacement refers to the physical damage to a crystal lattice produced by displacing an atom from its normal lattice position. Ionization is the freeing of orbital electrons from an atom to form ionized atoms and free electrons. Ionization is an intermediate process for both transient and surface effects of radiation and since the amount of ionization is proportional to the energy deposited for typical energies of nuclear radiation, the effects per rad are the same, no matter what radiation caused the ionization[27]. The typical transient effect is an electrical current that decays after a radiation pulse, while surface effects can persist for periods of years after the radiation exposure. Since displacement damage effects are produced by the disruption of the normal crystal structure in the bulk of a semiconductor device, this type of damage is sometimes called bulk radiation damage, particularly when discussed in relation to surface damage. The bulk and surface damage persist after the device is removed from the radiation field and appreciably affect transistor parameters. An understanding of the physical-electrical relationships is the basis of the technique by which the physical relationships of a specific

device are inferred from its electrical behavior. Changes in the impurity concentrations, minority carrier lifetimes, and carrier concentrations can be calculated for a given radiation exposure. In analyzing nuclear radiation damage, it is frequently necessary to calculate the effect of a mixed spectrum of neutrons and ionizing gamma radiation. There is considerable evidence[28-31] supporting the defect cluster model in the bulk material caused by fast neutrons (E>10 keV) in contrast to the ionizing radiation induced surface damage at low gamma doses $[(10^4$ to 10^6 rads (Si)$]$.

B. Effect of a Mixed Radiation Spectrum on Junction Capacitance

The p-n junction capacitance depends explicitly on the junction area and the space-charge concentration at the edges of the depletion layer. The ionizing gamma radiation present in the nuclear reactor will induce positive space-charge build up in the passivating layer above the p-n junction. This positive charge build up on the p type base, will cause inversion and channel formation, thus increasing the effective junction area and the capacitance. The fast neutron-induced carrier removal caused an increase of the depletion layer width and hence a decrease in capacitance. The simultaneous effect of ionizing gammas and fast neutrons on the junction capacitance variation is shown in Figure III-1. The collector-base junction capacitance versus total neutron fluence (E>10 keV) with measurement voltage as a parameter for an SF2523 silicon planar device is plotted in Figure III-1 from the data[32] listed in Table III-1. The initial increase in the junction capacitance can be attributed to the gamma induced surface effects. The maximum value of capacitance is reached at a

TABLE III-1. Normalized collector-base junction capacitance for SF2523 device at different measurement voltages and neutron fluences (with accompanying gamma doses).

Neutron Fluence, neutrons/cm^2 Φ	Gamma Dose rads (Si) γ	16V Reverse (measurement) bias (capacitance) pf	0.8V Reverse (measurement) bias (capacitance) pf	Zero volts (measurement) bias (capacitance) pf
0	0	3.62	6.34	8.44
4.9×10^{12}	5.39×10^{4}	3.62	6.31	8.36
1.07×10^{13}	1.17×10^{5}	3.59	6.24	8.30
1.97×10^{13}	2.17×10^{5}	3.54	6.20	8.25
3.77×10^{13}	4.15×10^{5}	3.50	6.22	8.12
6.14×10^{13}	6.75×10^{5}	3.56	6.59	8.19
8.19×10^{13}	9.01×10^{5}	3.93	6.57	8.50
1.02×10^{14}	1.12×10^{6}	3.92	6.51	8.45
1.79×10^{14}	1.97×10^{6}	3.88	6.50	8.37
2.31×10^{14}	2.54×10^{6}	3.78	6.38	8.35
2.84×10^{14}	3.12×10^{6}	3.51	6.10	8.22
3.30×10^{14}	3.63×10^{6}	3.52	6.06	7.94
4.1×10^{14}	4.51×10^{6}	3.43	5.92	7.84

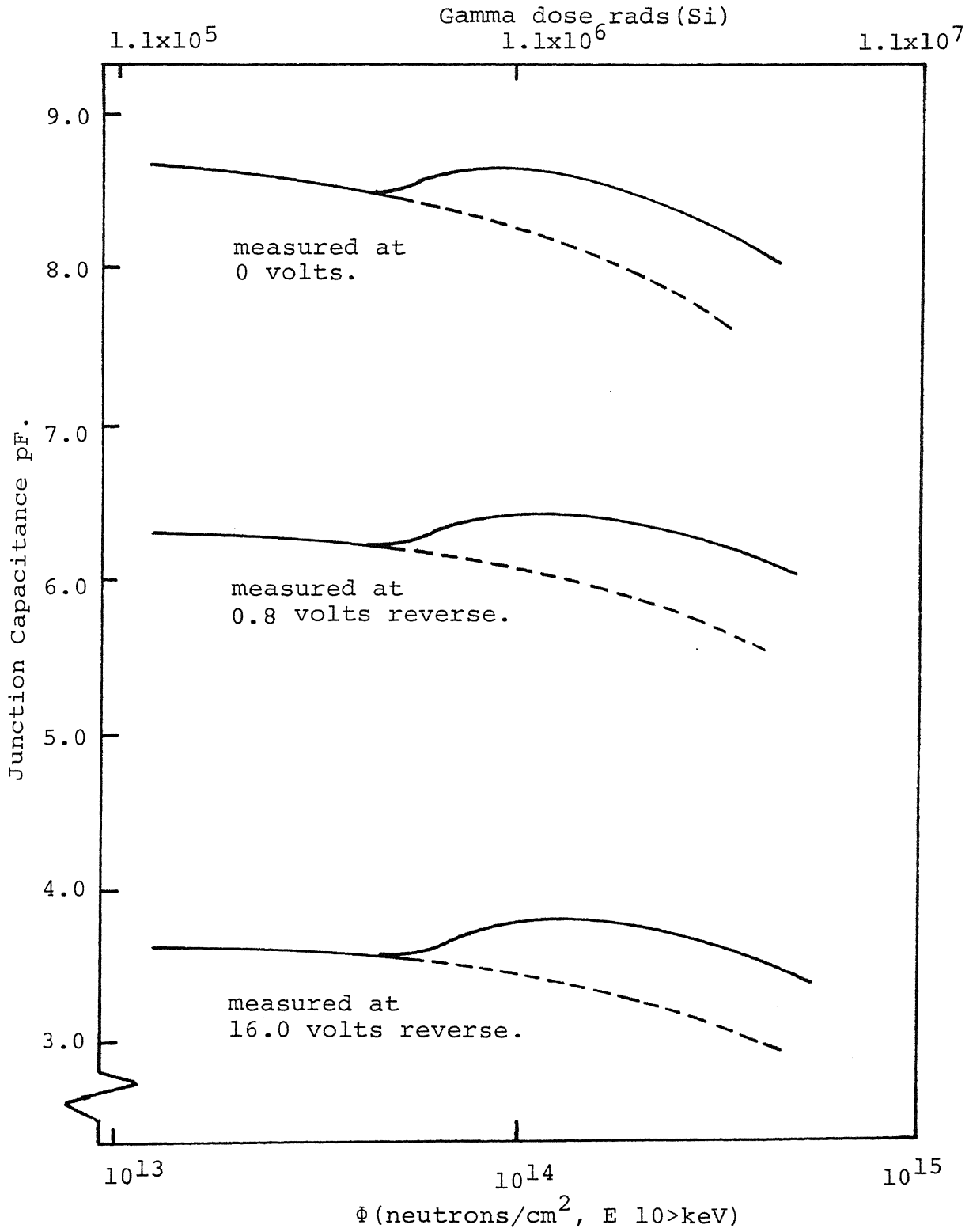

Figure III-1. Collector-base junction capacitance versus neutron fluence, before and after subtracting surface effects.

neutron fluence of about 10^{14} neutrons/cm^2, which corresponds to a dose of about 10^6 rads (Si), after which the surface effects are observed to saturate. Further irradiation beyond 10^{14} neutrons/cm^2, causes the junction capacitance to decrease, indicating the dominance of neutron induced carrier removal at higher fluences. The decrease in capacitance is attributed to the carrier removal by fast neutrons, which results in the increase in the depletion layer width. The thick lines in Figure III-1 are the junction capacitance changes for a combined field of neutron and gamma radiation. The broken curve indicates the junction capacitance change attributed to carrier removal by neutrons alone after the gamma induced capacitance increase has been subtracted. This technique of removing the effects of gamma induced surface effects is important when capacitance-voltage data is used in determining the impurity profile in the vicinity of the p-n junction at various neutron fluence levels[32]. Similar results were reported by Su et al.[12], who studied the effect of biasing the collector-base junction on the capacitance changes at low neutron fluences, where the gamma dose is the dominating factor in degradation of transistor characteristics.

C. Separation of Gamma and Neutron Induced Base Current Components

A nuclear radiation field of fast neutrons and gamma photons will induce several components of base current in a transistor. The observed increase in the base current is the sum of neutron-induced space-charge component, the neutron-induced neutral-base region recombination component and the ionizing radiation induced surface components of current. For calculating

the rate of space charge volume damage introduction, K_v, it is essential that the neutron-induced space-charge recombination current be accurately determined. This fraction of the total base current increase, $\Delta I_{B\Phi}$, which originates in the emitter-base space-charge volume[8-11] and is attributable only to neutrons, may be calculated over a wide range of currents by subtracting the gamma induced surface current component and the neutron induced neutral base region current component from the total current change.

The expression for this operation may be written as:

$$\Delta I_{B\Phi}(V_{BE}, E_r \Phi) = \Delta I_B(V_{BE}, E_r, \Phi, \gamma) - Z \cdot I_C(V_{BE}, \Phi) - I_{BO}(V_{BE}) \cdot f(V_{BE}, E_r, \gamma), \quad \text{(III-1)}$$

where,

ΔI_B = the measured total change in the base current caused by the introduction of the bulk space-charge recombination current plus the neutron-induced increase in the neutral-base recombination current and the gamma-induced surface current (amperes),

ΔI_C = the measured decrease in the collector current due to the neutron-induced increase in the neutral-base region recombination (amperes),

Z = ratio of increase in the neutral-base region current component to decrease in collector current (1.75 for the 2N914 devices studied)[10,33],

$I_{BO} \cdot f$ = empirical expression for the addition of surface currents in terms of the initial base current and the electric field strength present during irradiation[26,34].

The gamma induced surface current component, I_{SRG}, is introduced by the surface recombination generation of carriers by the "fast" surface states present at the intersection of the p-n junction and the oxide layer[4,5,25]. This separation is done using the equation II-1 (see Chapter II) relating the gamma-induced surface current to the initial base current and the field present during exposure[24,35] to ionizing radiation. The use of the expression derived for Cobalt-60 gamma dose-induced currents to remove the surface current component for this fission source is justified on the basis of the proximity of the average photon energies for the two sources[36].

D. Method of Calculating the Rate of Fast Neutron Induced Space-Charge Volume Damage Introduction

The fast neutron induced change in transistor parameters can be determined after taking into consideration the gamma induced surface effects. The rate of space-charge volume damage introduction, K_v, can then be determined from the expression[12,15]

$$\Delta I_{B\Phi} = K_v \cdot x_m(V_{BE}, \Phi) \cdot A_E \cdot \Phi \cdot \exp(qV_{BE}/nkT), \qquad \text{(III-3)}$$

where,

$\Delta I_{B\Phi}$ = space charge region neutron-induced base current component,

A_E = effective emitter area (cm^2),

K_v = rate of volume damage introduction (amperes$\cdot cm^{-3}/n\cdot cm^{-2}$),

Φ = neutron fluence (neutrons/cm^2, E > 10 keV),

q = electric charge (coulombs),

V_{BE} = base-emitter bias (volts),

n = reciprocal slope term $\simeq 1.5$,

k = Boltzman's constant (eV/^oK),

T = temperature (^oK),

x_m = base-emitter depletion layer width (cm).

The space-charge region neutron-induced base current component, $\Delta I_{B\Phi}$, is primarily responsible for degradation of silicon device current gain at low and intermediate current levels through degradation of the emitter efficiency. To determine the dependence of the rate of the space-charge volume damage introduction, K_v, on neutron fluence, the magnitude of the neutron-induced space-charge component of base current, $\Delta I_{B\Phi}$, the voltage dependence of this component (i.e., the reciprocal slope term, n), and the volume of the emitter-base space-charge region ($A_E \cdot x_m(V_{BE}, \Phi)$) must be determined.

Since the base current is composed of several current components [9-11,37], direct measurement of the neutron-induced space-charge component of base current over anything but a small portion of the device current-voltage character-

istics is not possible. At intermediate and moderate current levels the changes in only two base-current components dominate the total base current change. The first is the neutron-induced space-charge component and the second is the neutron-induced neutral-base region recombination component. It has been reported previously that the neutron-induced space-charge component dominates the base current changes at lower fluences and/or low current levels and that the neutron-induced neutral-base component dominates at higher fluences and/or high current levels[8-11,33]. (The above statement holds when the devices are irradiated in a neutron field alone.) The earlier experiments referenced[8-11] were performed at the Sandia Pulsed Reactor Facility (SPRF)[38,39] which has a very low gamma to neutron ratio. The University of Missouri-Rolla Research Reactor used in this group of experiments has a gamma to neutron ratio of 1.1×10^{-8} rads (Si)/n · cm^{-2}. Consequently, it is necessary to remove the gamma-induced surface current from the base current changes in order to study the bulk effects. (This has been shown in Section III-C.)

The reciprocal slope term, n, has been determined previously for neutron irradiated devices and was found to vary for $0.15 \text{ eV} < |E_i - E_R| < 0.35 \text{ eV}$, as:[32,40]

$$\frac{1}{n} = 0.4107 + \frac{kT}{q} \cdot \frac{1.21 \times 10^{-3}}{V_T(\Phi) - V_{BE}} + \frac{kT}{q} \cdot \frac{2.948}{E_i - E_R} + 6.34 \times 10^{-3} \cdot \ln\left[\left(\frac{\sigma_p}{\sigma_n}\right)^{1/2} + \left(\frac{\sigma_n}{\sigma_p}\right)^{1/2}\right] \qquad \text{(III-4)}$$

where,

V_T = the diffusion potential (volts),

E_i = the intrinsic Fermi energy (eV),

E_R = the defect energy (eV),

σ_n = the electron capture cross-section (cm^{-2}),

σ_p = hole capture cross-section (cm^{-2}),

n = the reciprocal slope term.

The emitter area, A_E, was obtained from the manufacturer and was verified by optical measurements. The depletion layer width was calculated after each irradiation from the capacitance voltage measurements using the expression:

$$x_m(V,\Phi) = \frac{\epsilon \epsilon_o A_E}{C(V,\Phi)} \qquad \text{(III-5)}$$

where,

C = corrected emitter-base junction capacitance (farads),

ϵ_o = permittivity of free space (farads/cm),

ϵ = relative permittivity.

The junction capacitance, as measured by a Micro-Instrument Digital Capacitance Tester[24] and corrected for socket and header capacitance, consists of the junction capacitance and the diffusion capacitance.

The neutron fluence dependence of K_v was then determined from (III-3) using (III-1), (III-2), (III-4), and (III-5).

IV. EXPERIMENTAL DETERMINATION OF THE NEUTRON FLUENCE AND ELECTRIC FIELD STRENGTH DEPENDENCIES OF THE RATE OF SPACE-CHARGE VOLUME DAMAGE INTRODUCTION

A. Experimental Procedure and Results

Measurements were made on a group of matched devices whose emitter-base junctions were biased differently to produce varying magnitudes of electric field strengths during neutron irradiation, to determine if the space-charge volume damage introduction rate, K_v, was dependent on the p-n junction electric field strength present during irradiation. Initially three matched Motorola devices (See Table IV-1) were irradiated simultaneously in one step to a neutron fluence of 1×10^{14} neutrons/cm^2 (E>10 keV) and a gamma dose of 1.1×10^6 rads (Si), as a quick check for the existence of an electric field strength dependence. The collector current, base current, and junction capacitance were measured versus voltage after irradiation and K_v was calculated (at 500 mV forward bias) by the method discussed in Chapter III-D for each of the matched devices. The resultant rates of volume damage introduction are plotted as a function of junction electric field strength during irradiation in Figure IV-1 and show clearly that K_v is indeed affected by the magnitude of the junction electric field; K_v is observed to be an increasing function of the electric field strength.

The reciprocal of the junction capacitance (and accordingly the emitter-base depletion layer width) was found to be an increasing function of neutron fluence for fluences above 1×10^{14} neutrons/cm^2. This was attributed to a neutron-induced carrier removal phenomenon whereby the device net impurity profile is altered, thereby affecting junction parameters[32,40]. Since the deple-

TABLE IV-1 Listing of test devices and experimental conditions for fast neutron irradiation experiments.

Device Code	Number	Manufacturer	Au Doped	Average Total Field (volts/cm)$^{\alpha}$
2N914	11*	Motorola	Yes	1.13×10^5
2N914	16*	Motorola	Yes	3.90×10^4
2N914	32*	Motorola	Yes	1.20×10^4
SA7472	79^{+}	Texas Inst.	No	1.26×10^5
SA7472	45^{+}	Texas Inst.	No	4.61×10^4
SA7472	24^{+}	Texas Inst.	No	2.71×10^4
SA7472	25	Texas Inst.	No	2.50×10^5
SA7472	18	Texas Inst.	No	1.00×10^5
SA7472	15	Texas Inst.	No	1.30×10^4

* Three "off-the-shelf" Motorola 2N914 Transistors, whose junction capacitance at zero bias and collector and base currents over V_{BE} range of 0.2 to 0.7 volts were matched to within 10%.

$^{+}$ Three specially fabricated Texas Instruments devices similar to the 2N914, but without gold doping, whose junction capacitance at zero bias and collector and base currents over a V_{BE} range of 0.2 to 0.7 volt were matched to within 5%.

α All neutron irradiations were performed at the University of Missouri-Rolla 200 kW swimming pool reactor. A double walled aluminum sample chamber was used to hold the devices. The inner space of the chamber is filled with boron carbide, to allow only fast neutrons (E>10 keV) to bombard the devices. A gamma flux of 1.6×10^4 rads (Si) sec^{-1} is obtained with a fast neutron flux of 1.4×10^{12} neutrons cm^{-2} sec^{-1}.

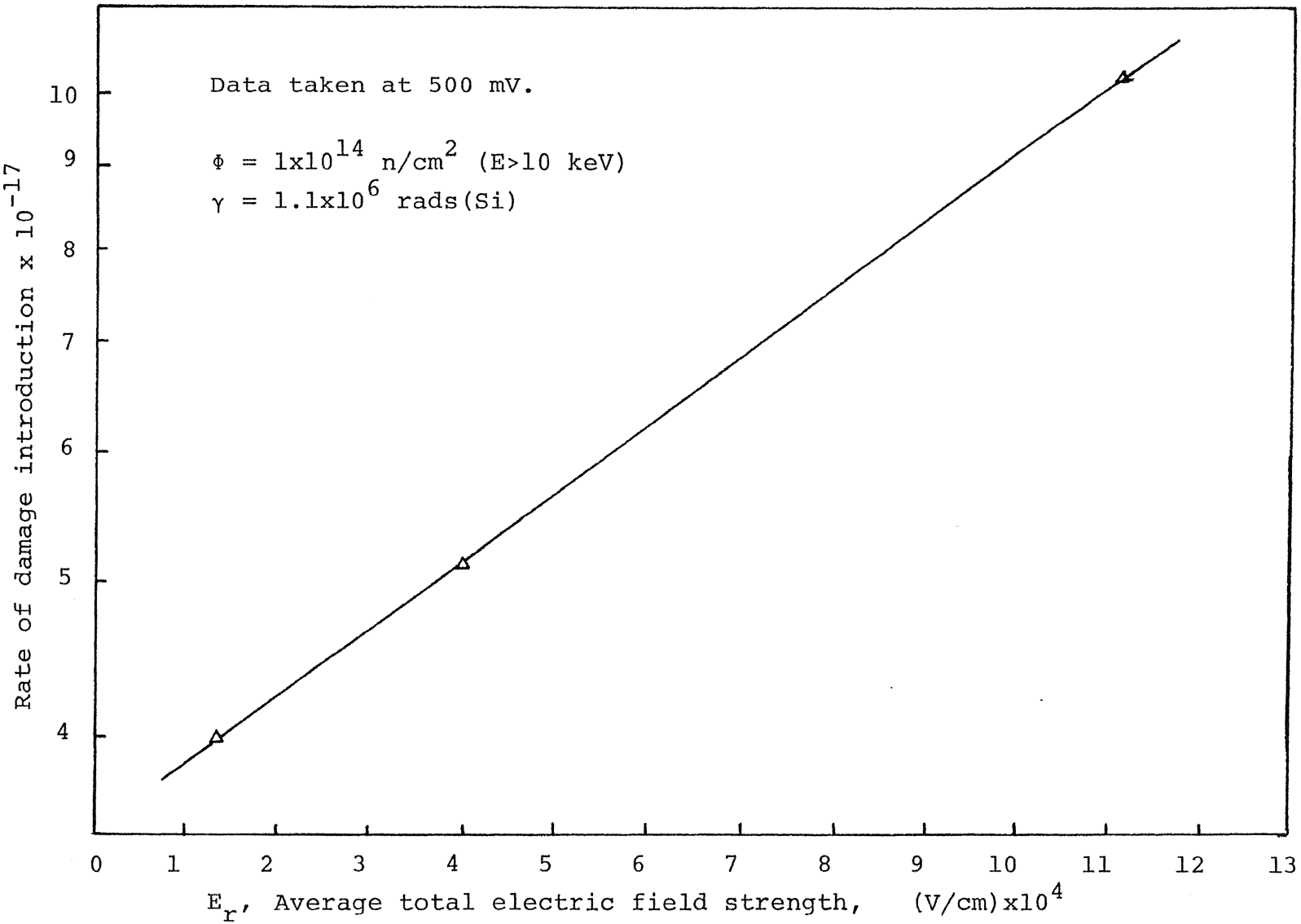

Figure IV-1. The rate of damage introduction versus average junction electric field strength present during neutron irradiation of matched Motorola 2N914 transistors.

tion layer width, x_m, is directly dependent on applied junction bias, the x_m's for four devices each at different biases were normalized to their preirradiation value to remove the voltage dependence. The normalized values were then averaged in order to establish the relative variation of x_m with neutron fluence which is shown in Figure IV-2. This plot indicates that the effective depletion layer width (at any particular bias) increases with increasing fluence, especially for fluences above 1×10^{14} neutrons/cm^2 (E>10 keV). Hence, we would expect K_v to be a decreasing function of neutron fluence.

Further experiments were conducted on six of a group of special devices fabricated by Texas Instruments, to fully determine the junction electric field strength and neutron fluence dependencies of the space-charge region rate of volume damage introduction. These devices were irradiated to a total fluence of 1.1×10^{15} neutrons/cm^2 (E>10 keV) in 28 steps. Capacitance-voltage and current-voltage data were taken after each irradiation step and the rate of volume damage introduction computed (at 500 mV forward bias) by the method previously discussed.

It is of interest to examine the current-voltage characteristics of the three matched devices, one of which was forward biased, one unbiased, and the other reverse biased during irradiation, corresponding to average junction electric field strengths of 2.7×10^4 volts/cm, 4.6×10^4 volts/cm and 1.26×10^5 volts/cm., respectively. Current-voltage characteristics for this set of devices at a fluence of 1×10^{15} neutrons/cm^2 (E>10 keV) are shown in Figure IV-3. The collector current is found to be invariant with the emitter-base junction field

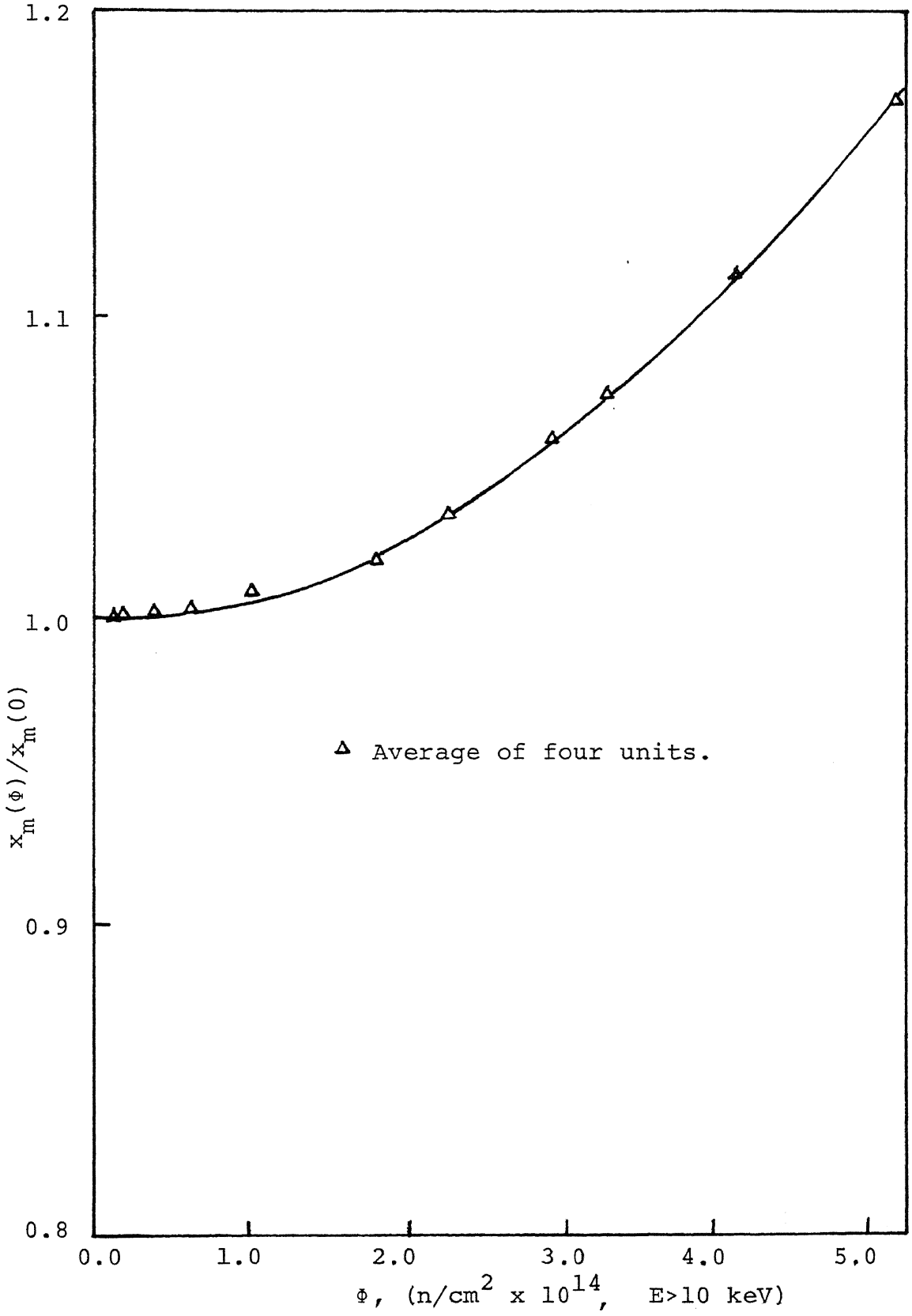

Figure IV-2. Normalized emitter-base depletion layer width versus neutron fluence.

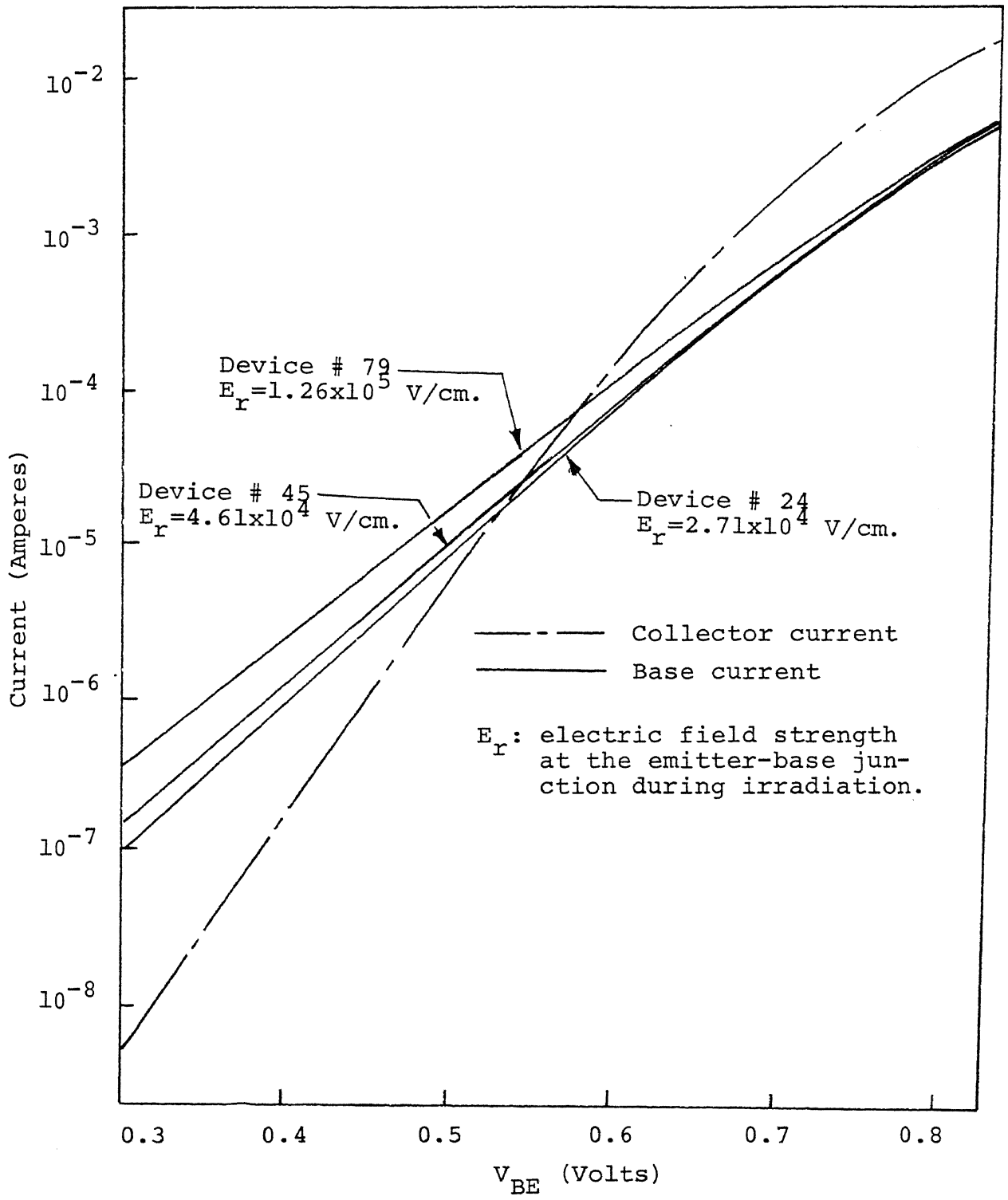

Figure IV-3. Current versus voltage for specially fabricated TI devices at different electric field strengths at the emitter-base junction during irradiation.

strength existing during irradiation. This should be expected since the collector current would be affected only by recombination in the neutral base region. The base current depicted in Figure IV-3 is observed to vary with the junction electric field strength existing during irradiation. From the slope of the base current at intermediate current levels, this variation can be seen to be dominated by changes in the neutron-induced space-charge region recombination current component rather than by surface effects. It should be noted here that the data in Figure IV-3 is for a relatively high neutron fluence and surface effects (which have saturation characteristics such that bulk damage dominates at higher fluences) would not be detected easily at this fluence by a "slope change" since the gamma-induced surface effects begin to saturate at $1 - 2 \times 10^{5}$ rads (Si), corresponding to $\sim 1 - 2 \times 10^{13}$ n/cm^{2}, and are completely saturated at 10^{6} rads (Si), corresponding to $\sim 10^{14}$ n/cm[26,35]. The recombination in the emitter-base space-charge region is observed from Figure IV-3 to increase with increasing electric field strength indicating that the severity of neutron-induced recombination at higher fluences in the space-charge region of an operating device is governed by the magnitude of the electric field present in the p-n junction during irradiation.

The values for the rate of volume damage introduction at various neutron fluences and junction electric field strengths are given in Table IV-2. $K_{V}(\Phi)$, the damage rate attributable only to neutrons is calculated after subtracting the surface component current from $I_{B}(\Phi,\gamma)$. Figure IV-4 is a plot of the rate of volume damage introduction versus neutron fluence. Interestingly, the introduction rate is accelerated for low fluences at high fields. It should be emphasized

TABLE IV-2 Calculated values of $K_v(\Phi,\gamma)$ and $K_v(\Phi)$ for matched SA7472 devices at various neutron fluences and at different average electric field strengths, E_r, during irradiation.

Neutron Fluence Φ neutrons/cm^2 E > 10 keV	Device #79 E = 1.26 x 10^5 V/cm		Device #45 E = 4.61 x 10^6 V/cm		Device #24 E = 2.71 x 10^6 V/cm	
	$K_v(\Phi,\gamma)$ x 10^{+17}	$K_v(\Phi)$ x 10^{+17}	$K_v(\Phi,\gamma)$x10^{+17}	$K_v(\Phi)$x10^{+17}	$K_v(\Phi,\gamma)$x10^{+17}	$K_v(\Phi)$x10^{+17}
1.0 x 10^{13}	170.0	131.0	40.0	31.3	12.0	----
3.0 x 10^{13}	73.6	59.1	24.6	16.3	11.6	----
5.0 x 10^{13}	50.5	39.2	19.6	12.7	11.0	----
7.0 x 10^{13}	39.5	31.1	15.7	10.2	10.4	----
9.0 x 10^{13}	33.3	27.0	14.1	9.8	9.7	0.14
1.0 x 10^{14}	30.1	24.1	13.4	9.4	9.5	0.50
2.0 x 10^{14}	18.9	15.7	9.6	7.6	7.7	3.36
3.0 x 10^{14}	14.8	12.7	8.2	6.9	6.8	3.70
4.0 x 10^{14}	12.6	11.1	7.4	6.4	6.2	3.90
6.0 x 10^{14}	10.4	9.4	6.6	6.1	5.8	4.30
8.0 x 10^{14}	9.3	8.6	6.2	5.8	5.5	4.48
9.0 x 10^{14}	8.7	8.1	6.1	5.7	5.4	4.48
1.0 x 10^{15}	8.6	8.0	6.0	5.6	5.3	4.47

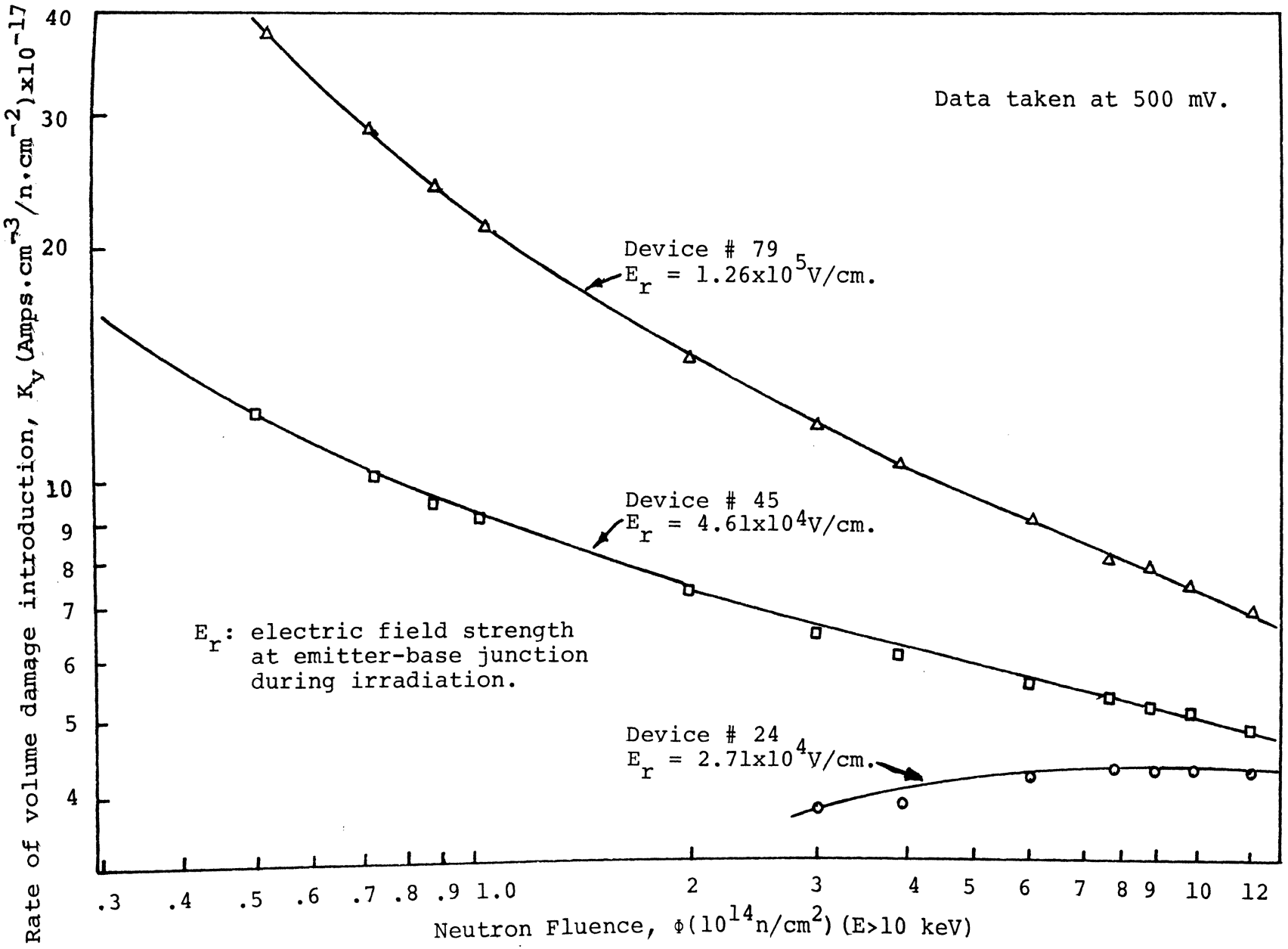

Figure IV-4. Rate of volume damage introduction versus neutron fluence for specially fabricated TI devices at different bias conditions.

that the data in Figure IV-4 represent only the neutron-induced recombination in the emitter-base bulk space-charge region as the neutron-induced recombination in the "neutral" bulk base region and the gamma-induced surface components have been removed as indicated by equation (III-1).

At higher fluences, K_v is a slowly decreasing function of fluence and continues to demonstrate a dependence on junction electric field strength (bias) during irradiation. This dependence could be attributed to injection annealing during irradiation, especially when the device is forward biased. This could possibly explain the inconsistency in K_v for low fluence conditions, but only for the forward biased device. If this dependence were indeed due solely to injection annealing, then the rate of volume damage introduction for the zero bias and reverse bias conditions should be identical for all practical purposes. This is not the case for the data presented in Figure IV-4 where the K_v's for the zero and reverse biased cases are seen to differ markedly even at very high fluences. The current density was computed for the forward biased device (#24-500 mV, 1 μA) and was found to be on the order of 10^{-2} amperes/cm^2 (injection ratio~10^{-4})[14]. Therefore, defect annealing caused by injection on the base side of the emitter-base space-charge region was considered to be non-negligible for the forward biased case. However, the behavior at zero and the reverse biases suggests that there must exist some other type of mechanism other than injection annealing which is responsible for the observed field dependence.

A plot of the rate of volume damage introduction versus the average total junction electric field strength present during irradiation with neutron fluence

as a parameter for the specially fabricated matched devices is illustrated in Figure IV-5. Note that for higher fluence levels, K_v follows a power law relationship with junction electric field strength. At lower fluences, the magnitude of K_v is larger and is influenced to a greater extent by junction electric field strength variations. At higher fluences, K_v is smaller and is affected less by the electric field strength variations and assumes a simple power law dependence. An approximate expression for K_v as a function of neutron fluence and junction electric field strength during irradiation has been obtained from the data for fluences in the range from 2×10^{14} to 1×10^{5} neutrons/cm^2 ($E > 10$ keV) and junction electric field strengths between 10^4 and 10^5 V/cm having the form[34]

$$K_v = K_{vo} \cdot \left(\frac{\Phi}{\Phi_o}\right)^{-m(E_r)} \qquad \text{(IV-1)}$$

where

$K_{vo} = 4.48 \times 10^{-17}$ (A · cm^{-3}/n · cm^{-2})

$\Phi_o = 4.2 \times 10^{15}$ (n · cm^{-2})

$m(E_r) = \left[0.648 \ln (E/2.71 \times 10^4)\right]^2$

E_r = Junction electric field strength present during irradiation (volts/cm).

The rate of volume damage introduction, K_v, for the zero bias case is in good agreement with previously determined "damage constants" at "normally encountered" fluences and junction field strengths[8, 11, 12, 15] but is larger for the high field strengths at all fluences and is much larger for lower fluences.

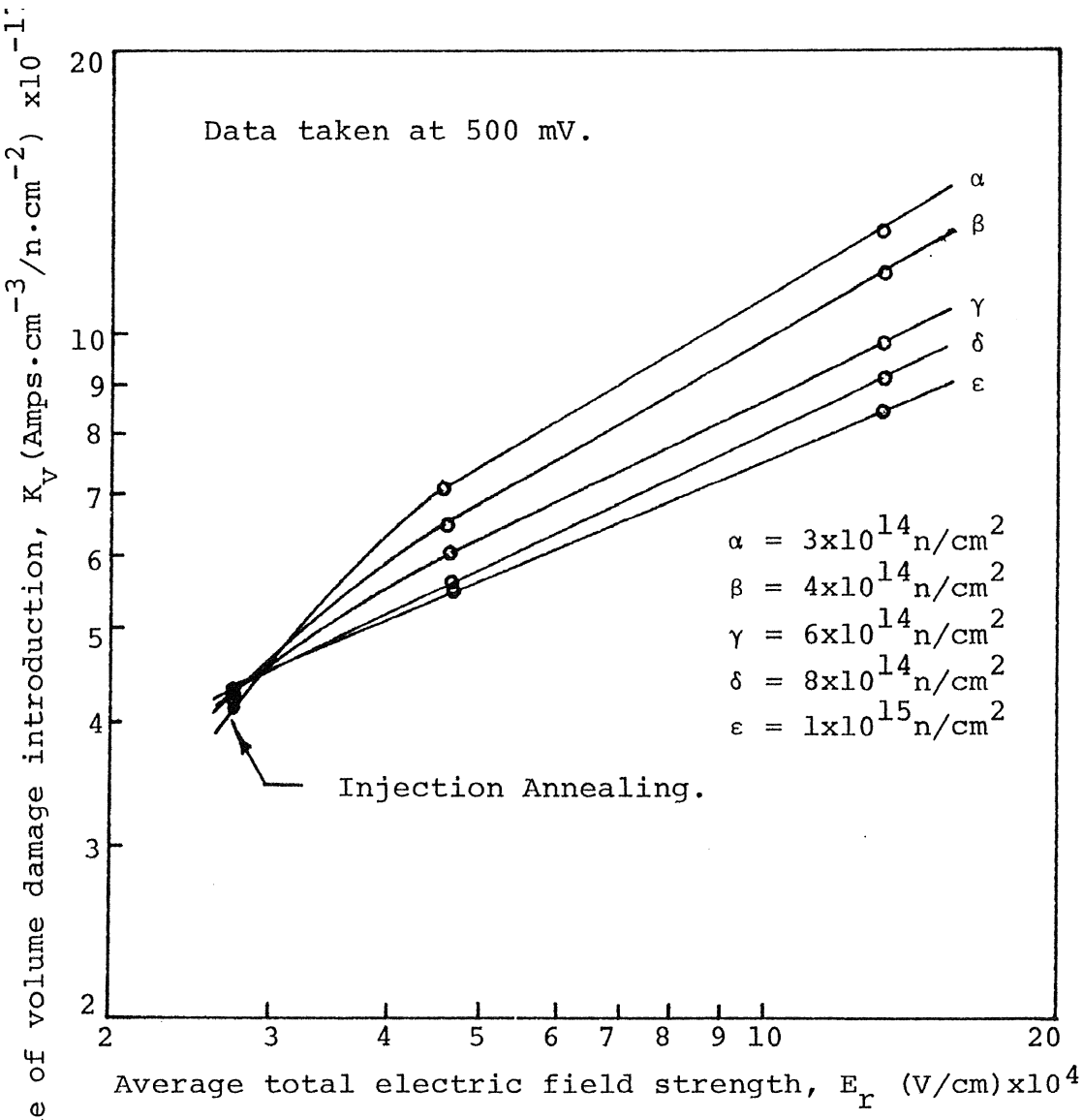

Figure IV-5. Rate of volume damage introduction versus average total electric field strength for specially fabricated TI devices at various neutron fluences.

B. Possible Mechanisms for the Field Dependence of the Rate of Volume Damage Introduction

The neutron fluence dependence of K_v, can be explained from the observed variance in the depletion layer width, x_m, since K_v is expressed as a function of x_m; $K_v = K_1/x_m$. Since the carrier removal and hence x_m increases with the total neutron fluence (E >10 keV), one would expect K_v to decrease with neutron fluence.

While the dependence of K_v on the neutron fluence is easily explained, the field dependence of K_v could be attributed to several possible mechanisms. It was noted (Figure IV-4) that the increase in K_v with the junction field strength present during irradiation is much more pronounced at low fluences than it is for high fluences. K_v is observed to decrease with increasing fluence at all levels except for the forward bias case at low fluences. This discrepancy from the general trend is felt to be caused by injection annealing[14]. Injection annealing during irradiation was considered as a possible mechanism for the junction electric field dependence, but it alone is unable to predict all of the observations since at zero and reverse bias the field dependence is quite pronounced. If injection annealing alone were responsible for the observed field dependence, then the reverse biased device should have a smaller rate of damage introduction, K_v, than the unbiased device. The experimental data did not follow this trend at all neutron fluences and this was enough to validate a conclusion that some other mechanism was responsible.

In Goben's previous work[8-11], it was reported that the annealing of neutron-induced defects in the high field space-charge region appeared to differ markedly from the annealing of defects in the low or zero field neutral base region. This suggests that these defects anneal differently due to the presence of the p-n junction electric field. In 1967 Chott and Goben[13] and in 1968 Su et al.[12] found that the annealing rate in the space-charge region (as reflected by the change in the base current component) was strongly dependent on the electric field at the junction during annealing and was attributed to the modification of the defect structure and/or properties of the neutron induced centers. The present investigation has shown the field dependence of the rate of volume damage introduction, K_v, which indicates that the defect cluster or its capture cross section is modified by the junction electric field[34].

V. MOBILITY OF NEUTRON RADIATION INDUCED DEFECTS IN SILICON P-N JUNCTIONS

A. Characteristics of the Si-E Center

The electrical and optical properties of defects introduced by high energy irradiation of semiconductors, particularily silicon and germanium, have been thoroughly investigated[41-47] and, although the energy levels are known in considerable detail, their identification in terms of structural defects is still under investigation. In silicon, a great improvement results from the use of electron spin resonance and elasto-plastic effects, which give a clearer picture of the association of vacancies with chemical impurities. (The "Si-E center" is the phosphorous-vacancy complex, and the "Si-A center" is the oxygen-vacancy complex.) In the present situation it seems important to investigate the motion and disappearance of Si-E centers, which are the dominant complex defects in irradiated phosphorous doped silicon with low oxygen content.[46,47] The Si-E center is formed when a vacancy drifts and is trapped next to a phosphorous atom. Because of the unpaired electron of the broken Si bond, an electron is captured and the center gets a net negative charge. Figure V-1 gives the model[46] of the Si-E center.

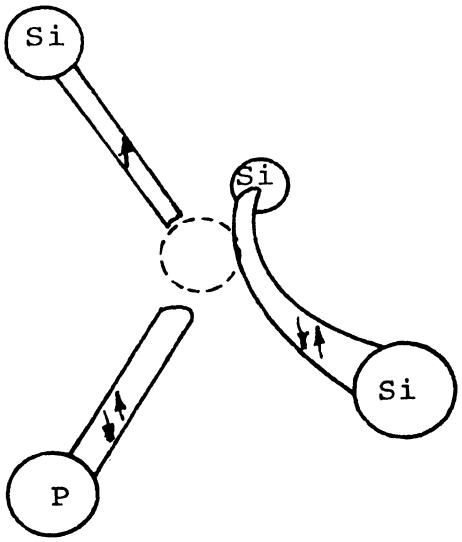

Fig. V-1 Model for the phosphorous-vacancy complex, the Si-E center.

The mobility of electron and gamma radiation induced point defects in the space-charge region of a p^+-n junction has been demonstrated in n-type germanium by Baruch[48] (1961) and in n-type silicon by Saltiel and Baruch[49] (1964). The dominant defect complex in phosphorous-doped float zone silicon was identified[46,47] as the phosphorous-vacancy pair (Si-E center) and was observed to be mobile in the presence of an electric field. The energy level of the Si-E center is generally observed to be 0.40 eV below the conduction band (E_c - 0.40 eV). Saltiel and Baruch[49] have shown that in n-type silicon (phosphorous-doped, resistivity 3 ohm-cm) the defect velocity is 3.6×10^{-9} cm/sec, corresponding to a mobility of defects of 1.8×10^{-14} cm^2/V-sec, and an activation energy of motion of (0.95 $\pm$ .02 eV). The above coefficients were obtained at a temperature of 70°C and a maximum electric field strength of 2.0×10^5 V/cm.

B. Field Sweeping Experiments and Results

In order to obtain a better understanding of the mechanism of the formation and annealing of fast neutron induced defects in the space charge region, the field sweeping of the defects after irradiation was studied. The test devices used were p^+-n junction diodes (silicon alloy) so that the depletion region extended almost entirely into the n-region when reverse biased (Hoffman 1N200 and 1N207 diodes). The devices were irradiated in steps up to 4×10^{14} neutrons/cm^2 (E >10 keV). Capacitance-voltage measurements before and after irradiation and after field-sweeping were made using the Micro-Instruments 1201DS Capacitance-Voltage Tester. After each irradiation step the devices were reverse biased in steps up to 70 volts (somewhat less than the breakdown voltage of the devices) and

simultaneously heated in an oil bath to temperatures up to 80^{o}C (the Si-E centers are known to anneal in the temperature range 100^{o}C to 120^{o}C). The oil bath consists of an aluminum container fabricated to hold 12 devices in one run. Special oils (polymethyl phenyl silicon fluids) were used. Table V-1 lists the typical capacitance-voltage reverse bias data obtained for an IN200 p^{+}-n diode at various stages of field sweeping.

The observed non-variance in capacitance values (see Table V-1) after the field sweeping process indicates that the defect concentration at the edge of the depletion layer (at zero and reverse biases) is apparently unchanged after field sweeping. It is important to note that the above data were reverse bias measurements, and hence will give no indication of the field sweeping of the defects in the immediate vicinity of the junction or within the depletion layer. Forward bias data is necessary to study the possible field sweeping in the junction region.

Recent investigations by Chow[16] revealed very interesting results from forward biased capacitance-voltage data taken from p-n junction diffused transistors which were irradiated with fast neutrons. Data taken on several devices, long periods (over 3 months) after irradiation revealed that the net impurity concentration in the vicinity of the junction increased as calculated from forward biased capacitance-voltage data, after removal of surface channels and diffusion capacitance. This increase was observed on both the p and n sides of the metallurgical junction. A possible explanation to this phenomenon could be given if one realizes that the average field strength in the junction is appreciable enough ($E \geq 5 \times 10^{4}$ V/cm) to cause the charged mobile defects to move out of the

TABLE V-1 Field sweeping data for device 1N200 #1.

Field Sweeping conditions →	Pre-irradiation	$\Phi = 1 \times 10^{14}$ n/cm^2	$\Phi = 1 \times 10^{14}$ n/cm^2 Temp. at 60°F for 24 hours	$\Phi = 1 \times 10^{14}$ n/cm^2 F.S. at 60°C, 20V for 48 hours	$\Phi = 4 \times 10^{14}$ n/cm^2	$\Phi = 4 \times 10^{14}$ n/cm^2 Temp. at 80°C for 48 hours	$\Phi = 4 \times 10^{14}$ n/cm^2 F.S. at 80°C, 70V for 64 hours
Measurement Voltage (Reverse) (volts)							
0.0	12.52	12.07	12.11	12.12	11.56	11.58	11.59
0.5	9.57	9.28	9.29	9.28	8.95	8.97	8.97
1.0	8.18	7.95	7.95	7.95	7.72	7.74	7.73
2.0	6.70	6.54	6.55	6.55	6.42	6.43	6.45
3.0	5.96	5.77	5.78	5.79	5.65	5.66	5.66
5.0	5.06	4.84	4.91	4.90	4.83	4.83	4.89

junction. Since this was observed on both sides of the junction, it can be postulated that at least two oppositely charged mobile defect complexes should exist.

VI. SUMMARY AND DISCUSSION

The first part of this research was the investigation of the electric field strength dependence of the rate of surface degradation in specially matched silicon planar transistors. It was found possible (for matched devices) to predict the gamma-induced surface leakage base current increase. Equation (II-4) is the empirical prediction equation for the normalized increase in base leakage current as a function of gamma dose (1×10^4 rads (Si) to 2.0×10^6 rads (Si)) and the average junction electric field strength (1×10^4 V/cm to 2×10^5 V/cm) at the emitter-base junction during irradiation. The effective minority carrier lifetime degradation can be related to the total gamma dose and the junction electric field strength given by equation (II-7), and is seen to follow a trend similar to (II-4). The rate of surface degradation, as reflected by the increase in the surface base current component, surface recombination velocity and junction capacitance is observed to be an increasing function of the electric field strength at the junction during exposure. This can be attributed to the junction fringing field dependence of the build up of positive charge and surface states in the SiO_2 layer above the space charge region.

The effect of a mixed spectrum of ionizing gammas and fast neutrons on transistor parameters was investigated. Surface effects caused by ionizing gamma radiation are a primary cause of damage at low neutron fluences for the swimming pool reactor used in these experiments. This is reflected by the initial increase in junction capacitance and the surface base current component. The gamma induced increase in junction capacitance (caused by surface channels) at 1×10^{14}

neutrons/cm^2 (which corresponds to a gamma dose of 1 x 10^6 rads (Si) had to be subtracted from the total junction capacitance to obtain the net decrease in capacitance caused by fast neutrons alone. The surface recombination base current, induced by the ionizing gamma dose and the neutron-induced base bulk current component had to be subtracted from the total observed increase in the base current before meaningful space-charge volume damage introduction rates could be calculated.

In an effort to explain the anomalous behavior of the neutron-induced defect clusters in the silicon p-n junction space charge region, the dependence of neutron fluence and junction electric field strength present during neutron irradiation was examined. Experimental data from matched SA7472 silicon planar transistors indicate that K_v is a decreasing function of neutron fluence, as would be expected since x_m is found to be an increasing function of fluence. K_v is also seen to be dependent on the junction electric field strength present during irradiation. The neutron induced recombination is much more pronounced for the higher junction electric field strengths present during irradiation for low fluences. From an analysis of the data presented in Figure IV-4, it is clear that the rate of volume damage introduction varies with the electric field strength present during neutron irradiation for all neutron fluences. It is noted that the increase in K_v with the junction field strength present during irradiation is much more pronounced at low fluences than it is for high fluences. K_v decreased with increasing fluence at all neutron fluences except for the forward biased case at low fluences. This discrepancy from the general trend was felt to be caused by injection annealing.

Injection annealing during irradiation was considered as a possible explanation for the junction electric field dependence but it alone was unable to predict all of the observations (zero and reverse bias cases). This was sufficient to conclude that some other mechanism was responsible for the observed damage introduction rate. The exact nature of the field dependence (whether the defect cluster or its capture cross section is modified by the junction electric field) could not be determined and further work in this area is needed (see Section VIII). The rate of space-charge region volume damage introduction was experimentally determined and found to be a function of both neutron fluence and the junction electric field strength present during irradiation rather than a constant, as thought earlier. An empirical expression was developed for K_v from data taken on specially fabricated devices. This expression gives reasonable predictions for fluences between 2×10^{14} and 1×10^{15} neutrons/cm^2 ($E > 10$ keV) and junction electric field strengths between 10^4 and 10^5 V/cm (ranges of fluences and fields were surface effects and injection annealing can be considered negligible or subtracted with reasonable accuracy for the type of devices tested).

The drift mobility of neutron induced Si-E centers in the p-n junction devices was investigated. From reverse bias capacitance-voltage data obtained, no apparent mobility of the Si-E center could be observed. Forward bias measurements made by Chow[16] have indicated an increase in the net impurity concentration near the vicinity of the junction for diffused transistors. This could be attributed to the field sweeping of the defects by the high field in the space charge region.

VII. CONCLUSIONS

This research has shown that the rate of bulk and surface damage introduction is dependent on the electric field strength through the bias applied to the device junctions during irradiation. In general, the rate of volume damage introduction, K_v, and surface degradation are seen to be an increasing function of the average electric field strength present during irradiation. At the present stage of development of this research the following specific conclusions can be made.

(1) The ionizing gamma dose induced surface degradation (as reflected by the increase in the surface base current component surface recombination velocity and junction capacitance) is observed to be an increasing function of the electric field strength at the junction during irradiation. For specially matched, oxide passivated silicon transistors, an empirical prediction equation of the form

$$I_B(V_{BE}, E_r, \gamma)/I_{BO}(V_{BE}) = K_s(E_r) \cdot \left\{1-\exp(-\alpha(E_r) \cdot \gamma)\right\} \qquad \text{(VII-1)}$$

has been obtained correlating the normalized increase in the surface base current component with the total gamma dose and the average junction electric field strength during irradiation. The empirical equation correlating the reciprocal minority carrier lifetime with the junction electric field strength and the gamma dose is

$$(1/\tau_B - 1/\tau_0) = K(E_r) \cdot \left\{1-\exp(\alpha(E_r) \cdot \gamma)\right\}. \qquad \text{(VII-2)}$$

(2) The ionizing radiation induced surface effects are non-negligible at low neutron fluences in the swimming pool type reactor used in the present investigation. The gamma induced surface channel component of capacitance and

surface recombination base current component must be subtracted from the total observed changes in capacitance and base current values, respectively, to obtain meaningful interpretation of the fast neutron induced parameter changes. Methods for doing this are presented.

(3) The rate of space-charge volume damage introduction, K_v, is found to be an increasing function of the average junction electric field strength and a decreasing function of the neutron fluence. An empirical equation of the form

$$K_v = K_{vo} \cdot \left(\frac{\Phi}{\Phi_o}\right)^{-m(E_r)} \qquad \text{(VII-3)}$$

correlating K_v with the field strength and neutron fluence has been developed, which gives reasonable predictions for fluences between 2×10^{14} and 1×10^{15} (neutrons/cm^2, E >10 keV) and junction electric field strengths between 10^4 and 10^5 V/cm.

VIII. FURTHER RESEARCH PROPOSED IN THESE AREAS

A. Surface Damage Studies

It is suggested that the present work in surface damage studies be extended to obtain a better understanding of the phenomenon involved. Work should be done in this direction and is briefly described below.

Empirical equations have been derived (Chapter II) which predict the increase in the normalized surface base current component and the surface recombination lifetime for minority carriers from studies of gamma irradiation on matched oxide passivated silicon transistors. These parameters have been observed to depend on the average junction electric field strength present during exposure and the total gamma dose. Similar studies should be performed on groups of unmatched devices. The search for a technique to predict surface degradation should be restricted to silicon devices with SiO_2 passivation, so that a basic theory for determining prediction techniques can be developed. Such a basic theory should point the way to more general techniques. Since the accumulation of surface states depends on initial conditions at the junction-SiO_2 interface, proper normalization techniques are essential for predicting transistor surface response to ionizing radiation.

The build up of positive charge in the SiO_2 passivation layer causes depletion and inversion in p-type semiconductor material and accumulation in n-type material. Hence, in a silicon n-p-n transistor the positive charge build up in the SiO_2 layer will cause depletion or inversion at both junctions in the p-type material. The impurity concentration in the immediate vicinity of the

junction at the surface and the applied junction bias determine the extent of depletion or inversion of the surface. Use of irradiation data on devices with the same surface concentrations and equivalent junction electric field strengths but with different surface areas should be irradiated to determine the area dependence of surface degradation. Devices with identical surface areas and equivalent junction electric field strengths but varying surface concentrations should be examined to determine their effect on ionizing radiation induced change in transistor parameters. Special gates diodes should be used to study the effect of gate bias on build up of positive charge in the oxide layer. A set of special n-channel and p-channel MOSFET's fabricated from the same silicon wafers should be obtained in order to facilitate the investigation of gamma-induced fast and slow surface states, channel conductance, surface inversion and noise problems. Such an investigation should lead to a successful prediction technique for the general case of unmatched devices operating in an ionizing radiation environment.

B. Space Charge Region Damage Studies

It is suggested that the present work in bulk space-charge damage studies to extended to obtain a better understanding of the phenomenon involved.

The anomalous behavior of neutron-induced defect clusters in the high field space-charge region, both during introduction and annealing has been shown to be dependent on the electric field strength in the junction, although no physical mechanism has yet been postulated. However, the nature of the defect clusters in bulk semiconductor materials has been characterized quite well.[28-31] Investigations of the neutron-induced defect structure in bulk semiconductors

have led to the postulation of a spherical low-density region of disorder surrounded by a space-charge region[29]. Gossick[29] and Cleland and Crawford[30] visualize this region as being depleted of charge carriers and acting essentially as an insulating void (defined by the screening distance in the medium), thereby limiting the local current flow. Gossick[29] alludes to a consideration of a change in the dielectric constant in his original work. The application of the Clausius-Mosotti determination for the relative dielectric constant gives the relation:

$$\epsilon = \epsilon_o \{ 3/(1-f) - 2 \}$$

where f is the volume of voids as given by:

$$f = \frac{4\pi}{3} r_{eff}^3 \times \text{Number Density},$$

and the increase in f in the space charge region would be reflected by the increase in ϵ. If this simple model for the polarizability applies, then a measurement of the dielectric constant should provide a sensitive means for determing the effect of the field on the formation of disordered regions and provide a better understanding of the field dependence of neutron induced defect clusters. Bertolotti[31] was able to photograph replicas of the defect regions in bulk semiconductor material and has shown that the neutron induced defects in his experimental samples were indeed spherical, as predicted by the Gossick model. The disordered region, which contains up to 10^5 atoms, has a radius of 150 to 200 Å. The screening distance of the space-charge region surrounding the disordered region should be greater than a Debye-Huckel length in the undistrubed lattice and may be written as

$$L_D = \left(\frac{1}{q}\right) \cdot \left(\frac{kT\epsilon}{N}\right)^{1/2},$$

where N is the carrier concentration, ϵ is the dielectric constant of the material and q, K and T have their usual meanings. In high resistivity material, L_D is several orders of magnitude greater than the inner radius and the size of the potential well will be dependent on the outer space-charge region.

It is proposed to extend the work of Bertolotti[31] to an investigation of the defect cluster and the nature of its geometry within the depletion region of a p-n junction. Moreover, a technique for examining the cluster formation by using the "contrasts" technique has been developed.[50] This technique, in conjunction with the Scanning Electron Microscope (SEM), should allow the investigator to examine clusters in sectioned samples without the complicating step of replication.

These investigations should lead to a better understanding of the nature of the defect cluster in the high field space-charge region of a p-n junction.

IX. REFERENCES

1. G. J. Brucker, W. J. Dennehy and A. G. Holmes-Siedle, "Ionization and Displacement Damage in Silicon Transistors," IEEE Transactions on Nuclear Science, NS-13;6, 188-196, 1966.

2. W. Poch and A. G. Holmes-Siedle, "A Prediction and Selection System for Radiation Effects in Planar Transistors," IEEE Transactions on Nuclear Science, NS-15;6, 213-233, 1968.

3. M. A. Littlejohn and R. W. Lade, "Influence of Co-60 Gamma Irradiation on the Surface and Bulk Recombination Rates in Silicon," IEEE Transactions on Nuclear Science, NS-14;6, 305-318, 1967.

4. H. L. Hughes, "Surface Effects of Space Radiation on Silicon Devices," IEEE Transactions on Nuclear Science, NS-12;6, 53-63, 1965.

5. D. L. Nelson and R. J. Sweet, "Mechanisms of Ionizing Radiation Surface Effects on Transistors," IEEE Transactions on Nuclear Science, NS-13;6, 197-206, 1966.

6. P. R. Measel and R. R. Brown, "Low Dose Ionization-Induced Failures in Active Bipolar Transistors," IEEE Transactions on Nuclear Science, NS-15;6, 224-231, 1968.

7. E. H. Snow, H. S. Grove and D. J. Fitzgerald, "Effects of Ionizing Radiation on Oxidized Silicon Surfaces and Planar Devices," Proceedings of the IEEE, 55;7, 1168-1185, 1967.

8. C. A. Goben and F. M. Smits, "Anomalous Base Current Component in Neutron Irradiated Transistors," IEEE Radiation Effects Conference, Seattle, Washington, 1964. Also: Sandia Laboratory (Albuquerque, New Mexico), (Publication), SCR-64-195, 1964.

9. C. A. Goben, "A Study of the Neutron-Induced Base Current Component in Silicon Transistors," IEEE Transactions on Nuclear Science, NS-12;5, 134-146, 1965.

10. C. A. Goben, F. M. Smits and J. L. Wirth, "Neutron Radiation Damage in Silicon Transistors," IEEE Transactions on Nuclear Science, NS-15;2, 14-29, 1968.

11. C. A. Goben, "Neutron Bombardment Reduction of Transistor Current Gain," Ph.D. Dissertation, Iowa State University Library (Ames, Iowa), 1965. Also: Sandia Laboratory (Albequerque, New Mexico), (Publication), SCR-64-1373, 1964.

12. L. S. Su, G. E. Gassner and C. A. Goben, "Radiation and Annealing Characteristics of Neutron Bombarded Silicon Transistors," IEEE Transactions on Nuclear Science, NS-15;6, 95-107, 1968.

13. J. R. Chott and C. A. Goben, "Annealing Characteristics of Neutron Irradiated Silicon Transistors," IEEE Transactions on Nuclear Science, NS-14;6, 134-146, 1967.

14. B. L. Gregory and H. H. Sander, "Injection Dependence of Transient Annealing in Neutron-Irradiated Silicon Devices," IEEE Transactions on Nuclear Science, NS-14;6, 116-126, 1967.

15. L. S. Su, "Radiation and Annealing Characteristics in Neutron Bombarded Transistors Operated in the Inverse Configuration," M. S. Thesis, Library, University of Missouri-Rolla, 1968.

16. M. C. Chow, "Recombination Statistics for the Neutron-Induced Base Current Component," Ph.D. Dissertation, Library, University of Missouri-Rolla, 1968.

17. G. Brucker, W. J. Dennehy and A. G. Holmes-Siedle, "High Energy Radiation Damage in Silicon Transistors," IEEE Transactions on Nuclear Science, NS-12;6, 69-71, 1965.

18. W. E. Horne and R. R. Brown, "Correlation of Electron-Induced Changes in Transistor Gain with Components of Recombination Current," IEEE Transactions on Nuclear Science, NS-13;6, 181-187, 1966.

19. R. R. Blair, "Surface Effects of Radiation on Transistors," IEEE Transactions on Nuclear Science, NS-15;6, 35-44, 1963.

20. D. L. Bartling, C. R. Jenkins and C. A. Goben, "An Automatic Data Acquisition System for Semiconductor Device Testing," IEEE Transactions on Instrumentation and Measurement, IM-17;1, 19-28, 1968.

21. D. L. Bartling, "An Automatic Data Acquisition System for Semiconductor Device Testing," M. S. Thesis, Library, University of Missouri-Rolla, 1967.

22. R. J. Maier, "Surface Effects on Transistors - Radiation Susceptibility of High Emitter Peripheral Arc Length Devices," USNRDL - TR -68-48, 29, March 1968, as cited by R. R. Brown, "Damage Constants for Surface Effects in Silicon Bipolar Transistors," Presented at IEEE Nuclear and Space Radiation Effects Conference, 1969.

23. Tektronix Type 555 Oscilloscope Manual, Tektronix, Inc. Beaverton, Oregon, 1964.

24. C. A. Goben, "Nuclear Radiation Effects on Silicon p-n Junctions," Technical Progress Report, Document C00-1624-11, Space Sciences Research Center, University of Missouri-Rolla, 1967.

25. C. T. Sah, "Effect of Surface Recombination and Channel on p-n Junction and Transistor Characteristics," IRE Transactions on Electron Devices, ED-9, 1, 94-108, January 1962.

26. C. A. Goben and C. H. Irani, "Prediction of Surface Effects in Silicon Transistors Caused by Gamma Radiation," to be Submitted to IEEE Transactions on Nuclear Science, 1970.

27. F. Larin, Radiation Effects in Semiconductor Devices, J. Wiley and Sons, Inc., New York, 2-5, 1968.

28. J. H. Crawford, "Radiation Effects in Semiconductors," reprinted from Interaction of Radiation with Solids, 121, (Plenum Press), 1967.

29. B. R. Gossick, "Disordered Regions in Semiconductors Bombarded by Fast Neutrons," Journal of Applied Physics, 30;8, 1214-1218, 1959.

30. J. W. Cleland and J. H. Crawford, "Nature of Bombardment Damage and Energy Levels in Semiconductors," Journal of Applied Physics, 30;8, 1204-1213, 1959.

31. M. Bertolotti, "Experimental Observation of Damage Clusters in Semiconductors," in Radiation Effects in Semiconductors, edited by F. L. Vook (Plenum Press), New York, pp. 311-330, 1968.

32. J. L. Azarewicz, "Calculation of the Neutron-Induced Changes in the New Impurity Concentration of Planar Epitaxial Transistors," presented at 8th Mid-America American Nuclear Society Conference, 1970.

33. J. Bereisa Jr., Unpublished Research, University of Missouri-Rolla, 1969.

34. C. A. Goben, C. H. Irani and P. E. Johnson, "Neutron Fluence and Electric Field Strength Dependencies of the Rate of Volume Damage Introduction in Silicon P-N Junctions," IEEE Transactions on Nuclear Science, NS-16;6, 43-52, 1969.

35. T. A. Niemeier, "Inversion Layer Growth by Gamma Radiation," Unpublished Research, University of Missouri-Rolla, 1969.

36. A. William Snyder, Sandia Laboratory, Albuquerque, New Mixico, Personal Communique, 1969.

37. A. B. Phillips, Transistor Engineering, McGraw-Hill Book Company, Inc., New York, 1962.

38. P. D. O'Brien, "Hazards Evaluation of the Sandia Pulsed Reactor Facility (SPRF)," Sandia Laboratory, SC-4357A (RR), 1961.

39. W. H. Buckalew, "Neutron Flux and Spectrum Measurements in the Sandia Pulsed Reactor Facility (SPRF)," Sandia Laboratory, SCR-463, 1962.

40. M. C. Chow, J. L. Azarewicz and C. A. Goben, "Recombination Statistics for Neutron Bombarded Silicon Transistors," IEEE Transactions on Nuclear Science, NS-15;6, 88-94, 1968.

41. G. D. Watkins and J. W. Corbett, "Electron Paramagnetic Resonance of Defects in Irradiated Silicon," Faraday Discussions, 31; 86, 1961.

42. G. D. Watkins, J. W. Corbett and R. M. Walker, "Spin Resonance in Electron Irradiated Silicon," Journal of Applied Physics, 30;8, 1198-1203, 1959.

43. G. D. Watkins and J. W. Corbett, "Defects in Irradiated Silicon-I: Electron Spin Resonance of the Si-A center," Physical Review, 121;4, 1001-1014, 1961.

44. J. W. Corbett, G. D. Watkins, R. M. Chrenko and R. S. McDonald, "Defects in Irradiated Silicon-II: Infrared Absorption of the Si-A center," Physical Review, 121;4, 1015-1022, 1961.

45. W. L. Brown and W. M. Augustniak, "Energy Orientation and Temperature Dependence of Defect Formation in Electron Irradiation of n-type Germinium," Journal of Applied Physics, 30;8, 1300-1309, 1959.

46. G. D. Watkins and J. W. Corbett, "Defects in Irradiated Silicon, Electron Paramagnetic Resonance and Electron Nuclear Double Resonance of the Si-E center," Physical Review, 134;5A, 1359-1377, 1964.

47. C. A. Klein, "Radiation-Induced Energy Levels in Silicon," Journal of Applied Physics, 30;8, 1222-1232, 1959.

49. E. D. Saltiel and P. Baruch, "Drift Mobility of Radiation Induced Defects in Silicon," 7th International Conference on Physics of Semiconductors, New York and London, pp. 275-280, 1964.

50. S. Kimoto and H. Hashimoto, "On the Contrast and Resolution of the Scanning Electron Microscope," Proceedings of the Symposium on the Scanning Electron Microscope - The Instrument and its Applications, Chicago, Ill., pp. 63-69, 1968.

X. ACKNOWLEDGEMENTS

The author acknowledges with profound gratitude the assistance rendered by Dr. Charles A. Goben, Senior Investigator (Materials), Space Sciences Research Center, in the accomplishment of this research effort.

The help rendered by several associates at the Materials Research Center and the personnel at the radiation facilities on the University of Missouri campuses at Rolla and Columbia is gratefully acknowledged. Special thanks are due to J. Bereisa Jr. and P. E. Johnson for their cooperation.

A note of thanks is extended to Texas Instruments and Motorola for fabrication of special devices used in this investigation and to the United States Atomic Energy Commission for their support of this research effort under contract AT(11-1)-1624.

XI. VITA

The author, Cyrus Hoshang Irani, was born on September 18, 1945 in Bombay, India. He received his primary and secondary education from St. Joseph's European High School, Bangalore, and graduated in 1962, passing the Senior Cambridge and European Secondary High School examinations with honors.

Mr. Irani attended the pre-degree courses at St. Xavier's College of the University of Calcutta and graduated in April 1963. He was then selected for admission to the Indian Institute of Technology, Bombay, in 1963 and graduated from that Institute, B. Tech (HONS), in April 1968. Mr. Irani was employed as a research assistant at Kirloskar Cummins Pvt. Ltd., Poona, India in the summer of 1967.

The author enrolled for the Master of Science Program in Nuclear Engineering in September 1968 at the University of Missouri-Rolla, and has (since that time) been working as a Graduate Research Assistant at the Graduate Center for Materials Research of the Space Sciences Research Center. He is a member of Sigma Xi and the American Nuclear Society.

APPENDIX A: AUTOMATIC DATA ACQUISITION SYSTEM AND DATA REDUCTION TECHNIQUES

1. General Description

An Automatic Data Acquisition System[A1] was used for the measurement and recording of the voltage versus current characteristics of the test devices. The system is capable of current and voltage measurement with an overall absolute accuracy of $\pm 0.3\%$ of reading in the range from 10^{-10} amperes to 2×10^{-1} amperes (over 9 decades). Figure A-1 shows a block diagram of the complete Data Acquisition System plus the additional facilities necessary for obtaining the V/I Characteristics. Figure A-1 also indicates the flow paths for data and control information between the various equipments. Figure A-2 is a photograph of the system as its operation is initiated.

The heart of this system is a Control Center[A2, A3] which controls the programming, measurement and recording sequence of the system. A signal is sent to the Programmer[A2, A3] to program the John Fluke 383B Voltage-Current Calibrator which applies an emitter-base bias to the test device which is mounted in a sample holder (see Figure A-3) contained within a Delta Design MK2310 Temperature Control Chamber. The collector-base bias is supplied by a manually controlled Harrison Labs 865C Power Supply or a digitally controlled John Fluke 383B Voltage/Current Calibrator. The currents are sampled by the Current Sampler[A2, A3] whose output is amplified by a low noise Sanborn Type 860-4300 amplifier and measured by a Dymec 2401C-M31 Digital Volt-

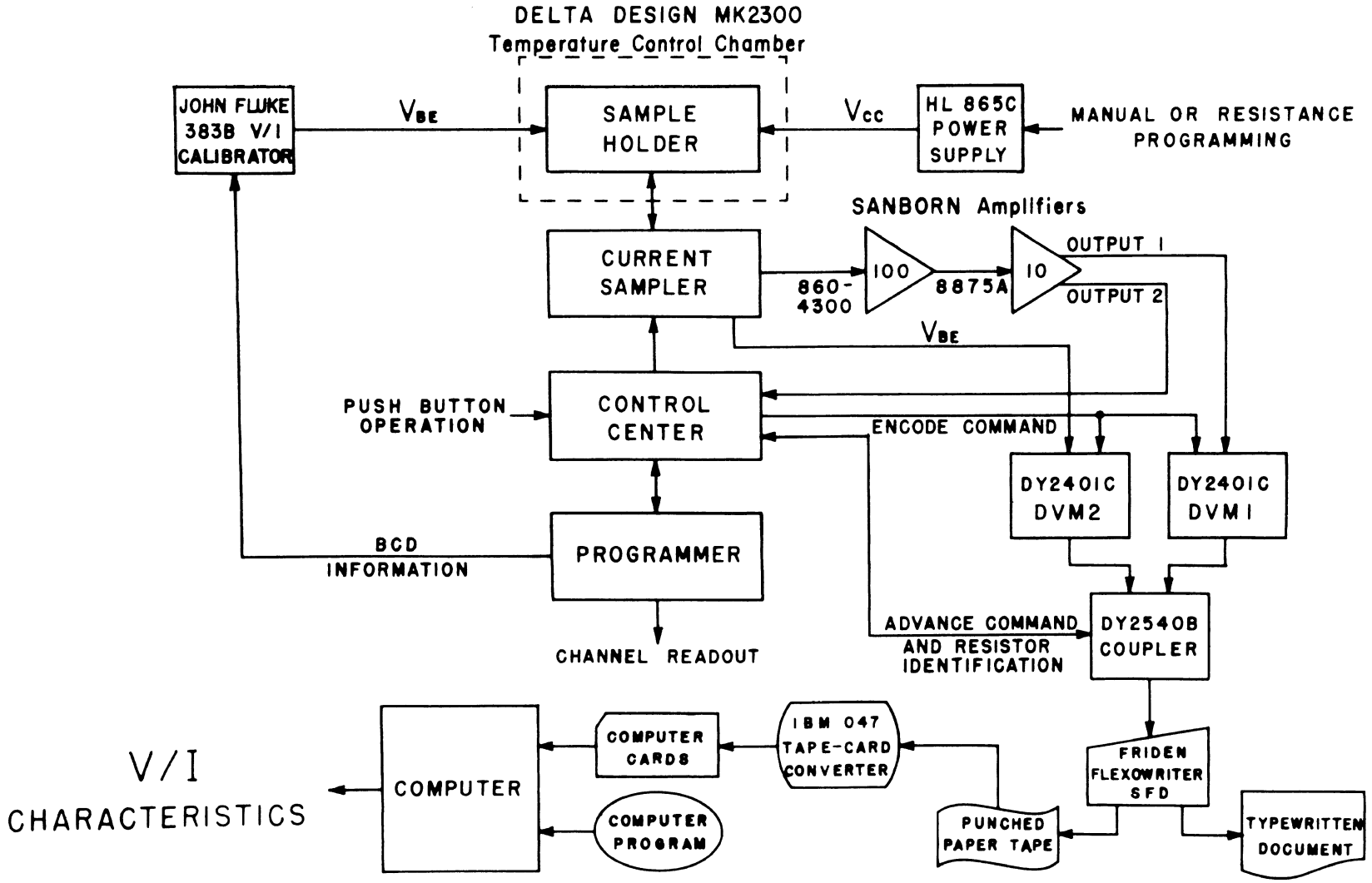

Figure A-1. Block diagram of the Automatic Data Acquisition System.

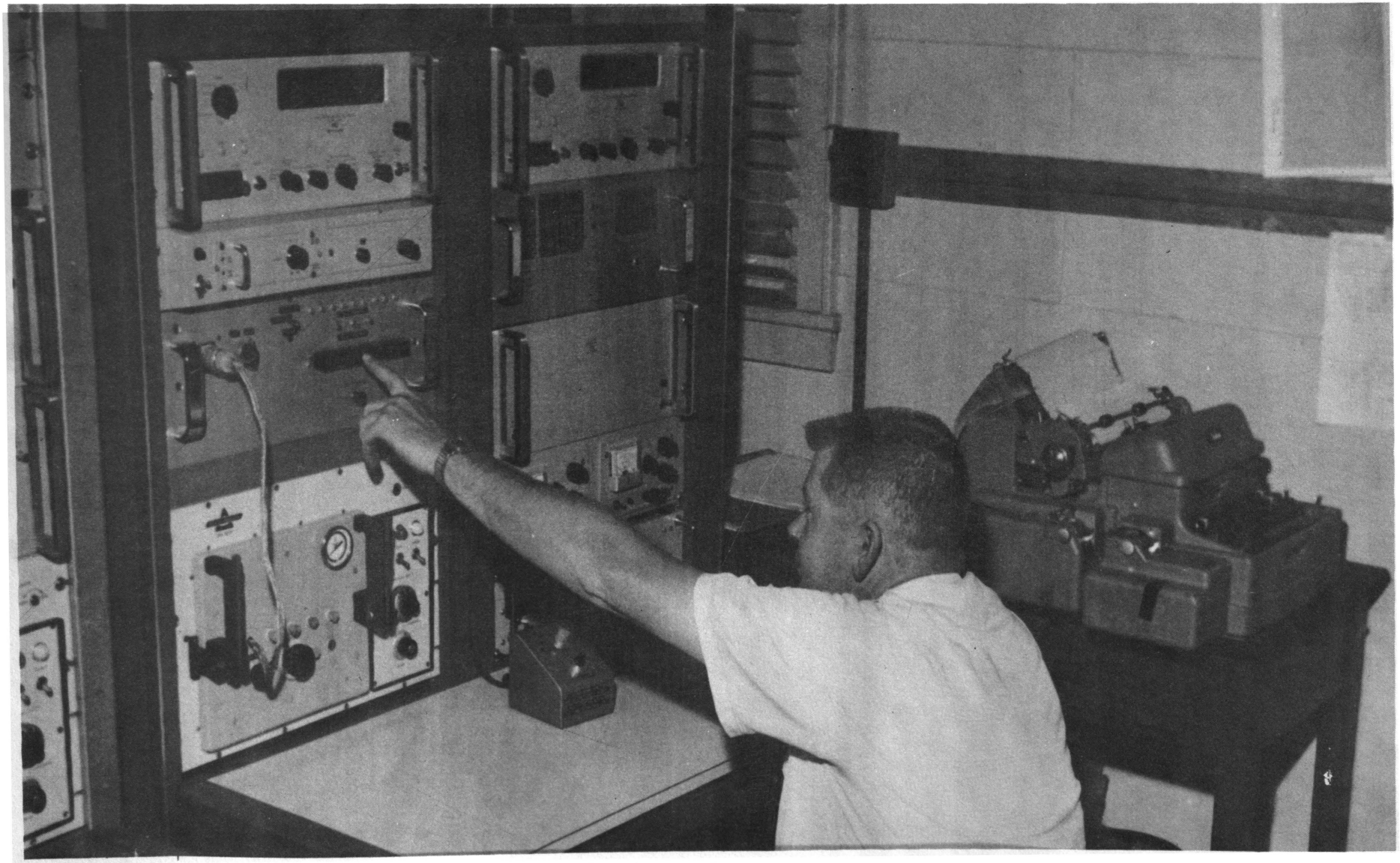

Figure A-2. Photograph of initiation of the system for a typical data run.

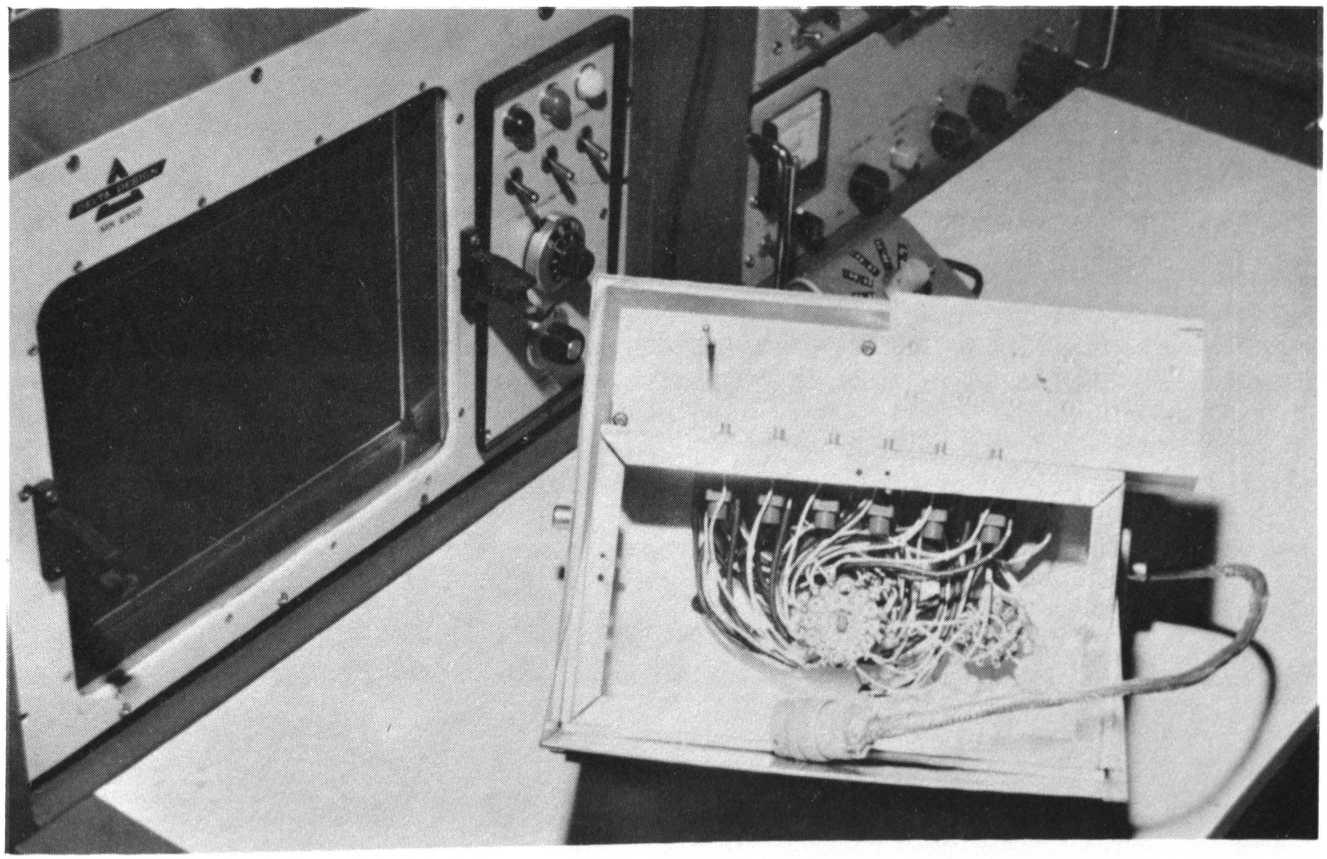

Figure A-3. Photograph of sample holder in its mounting, the heat sink standing behind the devices.

meter. The emitter-base bias voltage is measured by a second Dymec 2401C-M31 Digital Voltmeter. The voltmeter readings are recorded along with resistor identification information in digital form supplied by the Autoranging Current Sampler[A2, A3]. This information is serialized by a Dymec 2540B Coupler and recorded on a Friden Model SFD Flexowriter in both type-written form and on punched paper tape. The punched paper tape is converted to IBM punched cards on an IBM 047 Tape-to-Card Converter, and the punched cards are processed by an IBM 360-50 Digital Computer. The computer output is the tabulated voltage versus current characteristics and a plot (Calcomp Model 566) of the tabulated values.

A program has been written for the processing of the output data from the Automatic Data Acquisition System by the IBM 360-50 Computer. This program performs four major functions.

First, computation is made of device voltages and currents from the input voltage and resistance data with corrections made for the voltage drop across the current sampling element.

Second, interpolation is made to values of emitter-base voltage which are integral multiples of 10.0 millivolts. This interpolation provides a means of comparing currents and current gains at fixed values of base-emitter voltage.

Third, the applied base-emitter voltage versus base and collector currents and current gain is provided in tabular form together with heading information which includes device identification and measurement conditions.

Fourth, a machine plot (Calcomp Model 566) of input voltage versus logarithm of base current and logarithm of collector current, with printed device identification and neutron fluence, is returned for use by the investigator in comparison studies. Each plotted page is a 14 x 10 inch graph of the form log (I) versus V_{BE}. This particular program turns a plot of the logarithms of I_B and I_C versus V_{BE} for each device. A second plot program is available and returns one plotted page depicting either log (I_C) or log (I_B) versus V_{BE} curves for as many devices as desired.

The run time for the first plot program is approximately two and one-half minutes per device and the run time for the second plot program is approximately one minute per device.

The test device is located in the Sample Holder, as shown at the top of Figure A-1 which is, in turn, inside the Delta Design MK2300 Temperature Control Chamber. The MK2300 is a precision environmental temperature test chamber capable of maintaining any temperature from -297^{o}F (-196^{o}C) to 600^{o}F (+315.6^{o}C) within $\pm$0.1^{o}C. The forced air circulation system is closed and powered by a 140 CFM blower. The chamber is heated by applying full wave power to a pair of bobbin wound nichrome 720 watt heating elements controlled by the "heat" solid state switch. It has been suitably modified to be cooled by injecting liquid CO_2 or liquid N_2 into the air stream through an expansion nozzle controlled by the "cool" solid state switch.

Comparing the resistance of a temperature probe to the resistance of a "Temperature Set" potentiometer, the controller senses when to apply heat,

coolant, or withhold both so as to obtain and maintain a selected temperature in the chamber.

2. Cyclic Operation

The data for the base current versus voltage characteristic and collector current versus voltage characteristic is obtained with the device in, respectively, the Base Current Measurement Circuit shown schematically in Figure A-4, and the Collector Current Measurement Circuit shown schematically in Figure A-5. The Sampling Resistance appears in the measurement circuit as a physical resistance having one of nine discrete values, ranging from 17 milliohms to one megohm, each approximately a decade apart from the next. The Sampling Resistance is determined by the parallel combination of all resistors which are in the measurement circuit after the autoranging procedure is performed. The value of the Sampling Resistance as shown in Figure A-6 is, therefore, 17 milliohms.

The system is designed to perform a particular sequence of events in obtaining test data from a semiconductor device. In simplified terms, the sequence of events for one typical cycle of the system is as follows:

1. With the test device initially in the Base Current Measurement Circuit (Figure A-4) and with a particular value of base-emitter bias and collector supply voltage applied to the device, the system autoranges selecting one of the nine possible values of the Sampling Resistance such that the voltage drop across the Sampling Resis-

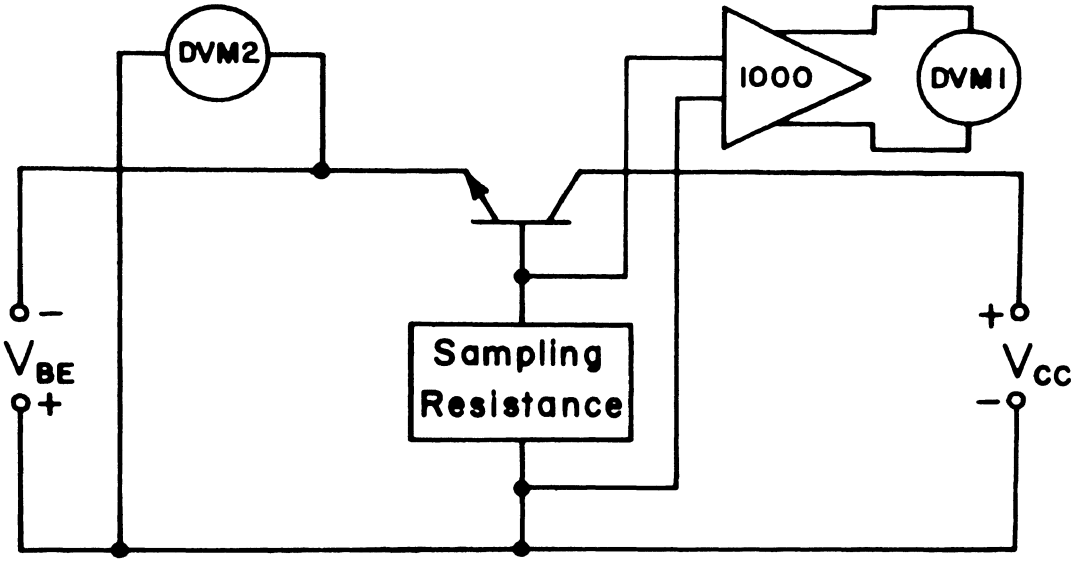

Figure A-4. Base current measurement circuit.

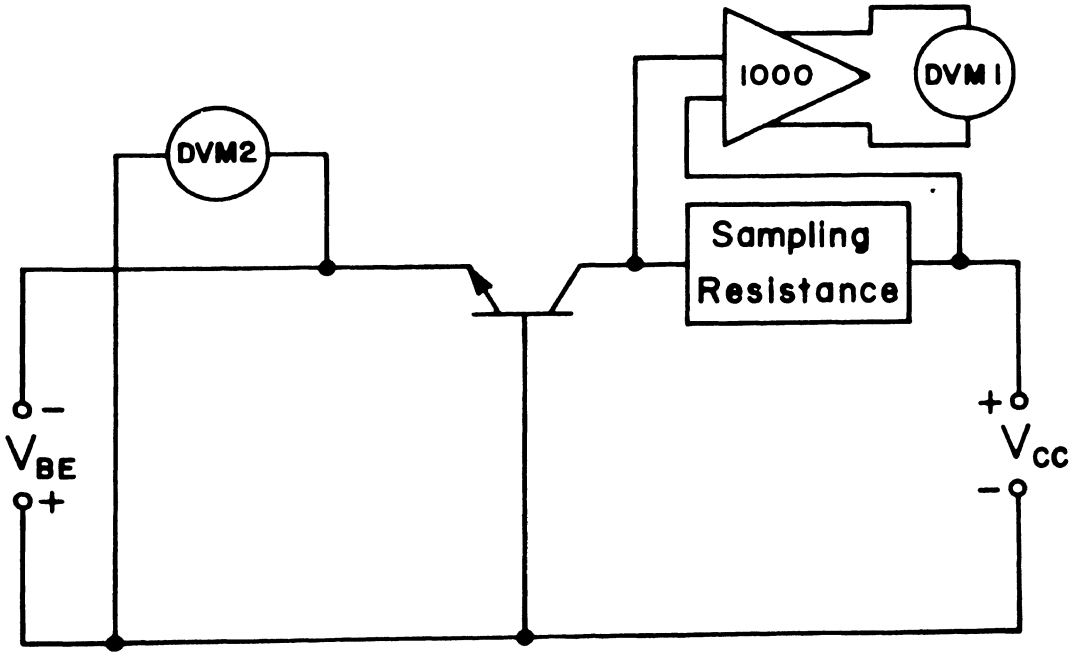

Figure A-5. Collector current measurement circuit.

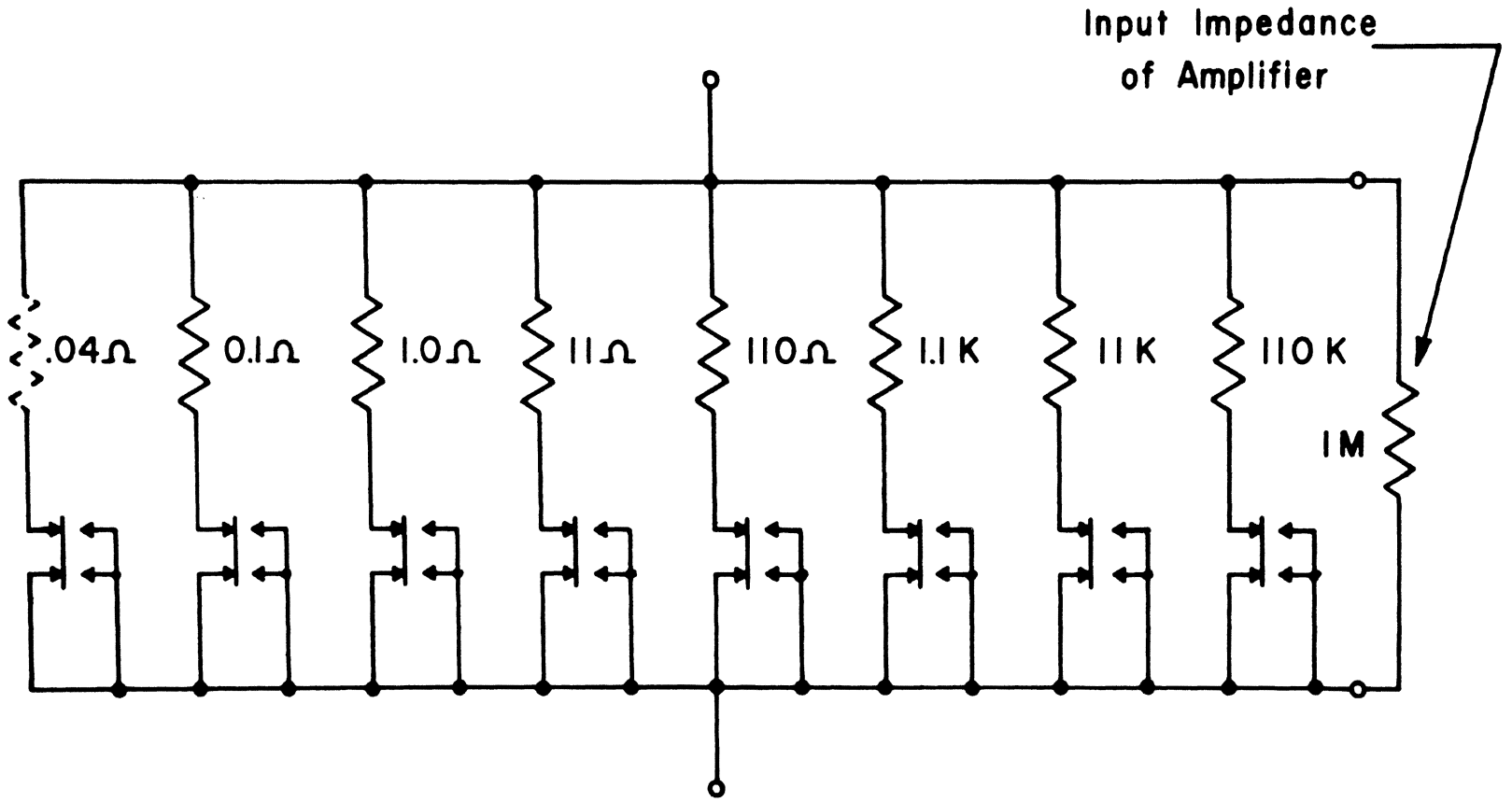

Figure A-6. Sampling resistance.

tance is normally greater than 0.5 millivolts and less than 5 millivolts. This autoranging procedure has been explained in detail in reference A2.

2. The digital voltmeters encode and their readings are recorded.
3. The device is switched into the Collector Current Measurement Circuit (Figure A-5).
4. The two digital voltmeters again encode and their readings are recorded.
5. The device is switched back into the Base Current Measurement Circuit (Figure A-4).
6. A new value of base-emitter bias, V_{BE}, is applied to the device and the sequence is repeated.

These steps define one cycle of the system. The system continues cycling in this manner until all of the required pre-programmed values of V_{BE} (59 values of V_{BE} are available if needed) have been used.

The collector supply voltage, V_{CC}, can be set manually before a test run in which case it remains constant during that test run, or a series of voltages can be programmed for a test run. In this second case, the emitter supply voltage, V_{BE}, is usually held constant.

An additional method of operation allows one to measure base current only or collector current only. This method of operation is selected by the MODE switch on the front panel of the control center.

A new feature of the system is the addition of an automatic stepping switch to allow taking data simultaneously on 12 devices in one data run. An interface is currently being designed and constructed which will allow the system to be controlled by a Digital Equipment Corporation PDP-8/I Programmed Data Processor. Controlling the system in this manner will provide more flexible system operation and enable some on-line data reduction. Recently, a switch has been installed which facilitates the application of a forward bias or reverse bias at the collector-base contacts for the n-p-n and p-n-p configurations. This allows for obtaining current versus voltage characteristics for both bipolar and MOSFET devices, with the system.

REFERENCES

A1. C. A. Goben, "Nuclear Radiation Effects on Silicon p-n Junctions," Technical Progress Report, Document COO-1624-24, Space Sciences Research Center, University of Missouri - Rolla, 1970.

A2. D. L. Bartling, "An Automatic Data Acquisition System for Semiconductor Device Testing," M.S. Thesis, Library, University of Missouri - Rolla, 1967.

A3. D. L. Bartling, C. R. Jenkins, and C. A. Goben, "An Automatic Data Acquisition System for Semiconductor Device Testing," IEEE Trans. on Instrumentation and Measurement, IM-17: 1, 19-28, 1968.

APPENDIX B: CAPACITANCE-VOLTAGE MEASURING SYSTEMS

Two systems were used for the measurement and recording of capacitance versus voltage data[B1]. The alternative capacitance measuring systems use a Micro-Instruments Model 1201DS Digital Capacitance Tester as the basic measuring instrument. A Dymec 2901A Master Scanner/Programmer and a Dymec 2902A Slave Scanner/Programmer are used for control and programming. The Dymec 2901A Master Scanner/Programmer and the Dymec 2902A Slave Scanner/Programmer are electronically controlled stepping switches which provide automatic scanning of 25 signal inputs each. The test devices in the alternative systems are mounted in a Delta Design MK2310 Temperature Control Chamber (see Appendix A).

The digital Capacitance Tester is a direct reading high speed instrument for accurate capacitance measurements. A guarded two terminal test jig is permanently attached to the front panel of the instrument. This test jig is guarded with a signal similar to the test signal to neutralize the capacitance effects of the component leads; thus, the instrument measures direct capacitance rather than grounded capacitance. Three BNC coaxial connectors for remote or special test jigs are provided on the front panel. The connectors provide for a test signal, a guard signal and a return for use with remote or special jigs. The Coarse Zero Control may be used to neutralize up to 100 pF of capacitance added by the cable and jig.

A digital output connector is provided on the Digital Capacitance Tester. This connector provides a print command signal as well as digital information to operate the Hewlett-Packard R66-562AR Digital Recorder. The recorder is controlled by means of a "Print" switch located on the front panel of the instrument. The output is BCD 1248 logic.

In the first alternative capacitance measuring system, a start command advances the scanner/programmer which digitally programs a voltage or current on a John Fluke 383B Voltage/Current Calibrator. This voltage or current is applied to the device under test. A capacitance reading is taken by a Micro Instrument Digital Capacitance Tester 1201DS and recorded on a Hewlett-Packard R66-562AR Digital Recorder together with the applied voltage which is measured by a Dymec 2401C-M31 Digital Voltmeter. The printed record is punched on IBM cards and processed by the IBM 360-50 Digital Computer. The block diagram for the system is shown in Figure B-1.

Alternatively, when the Automatic Data Acquisition System described in Appendix A is not in use for voltage-current measurements, the Dymec 2401C-M31 Digital Voltmeters, Dymec 2540B Coupler and Friden SFD Flexowriter may be used as the output medium. For this mode of operation the frequency output (proportional to capacitance) of the Micro-Instruments 1201DS Capacitance Bridge is measured by one of the DVM's in the Automatic Data Acquisition System while the other DVM measures the potential applied to the device under test. This information is then serialized by the Dymec 2540B Coupler and then printed as output by the Friden SFD Flexowriter on both punched paper tape and

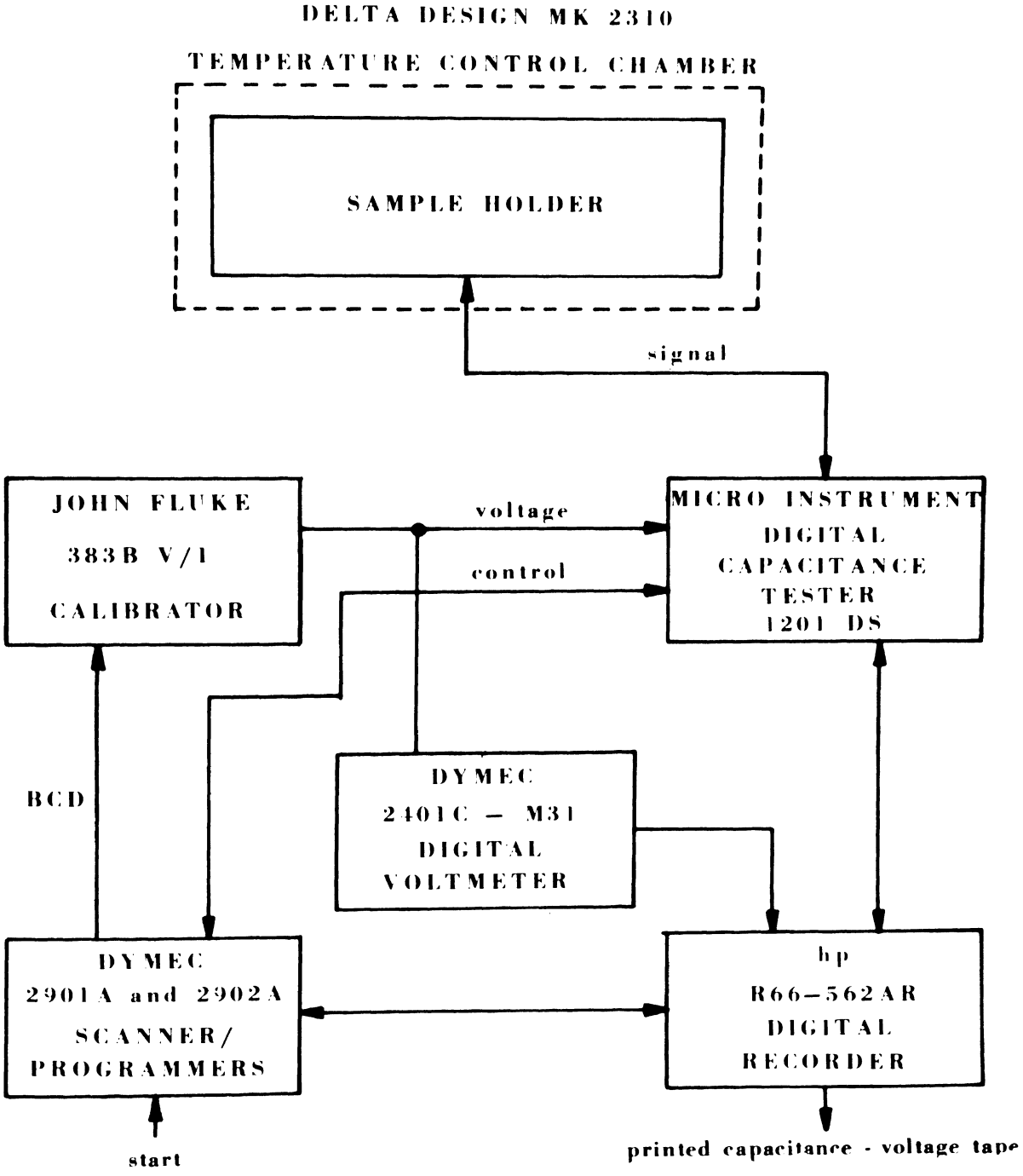

Figure B-1. Capacitance-voltage measurement system.

and typewritten copy. Data processing is accomplished in a similar manner to that described for the Automatic Data Acquisition System. The block diagram of the alternative system for the capacitance-voltage measurements is shown in Figure B-2.

To facilitate the inter-connection of the Automatic Data Acquisition System and the Capacitance-Voltage System for this alternative mode of operation, a single cable was constructed carrying all data, control and signal lines. When the two systems are used separately, shorting plugs are placed over the chassis connectors on the two systems.

This system will also be interfaced to the PDP - 8/I Programmed Data Processor to provide increased system flexibility and on line data processing.

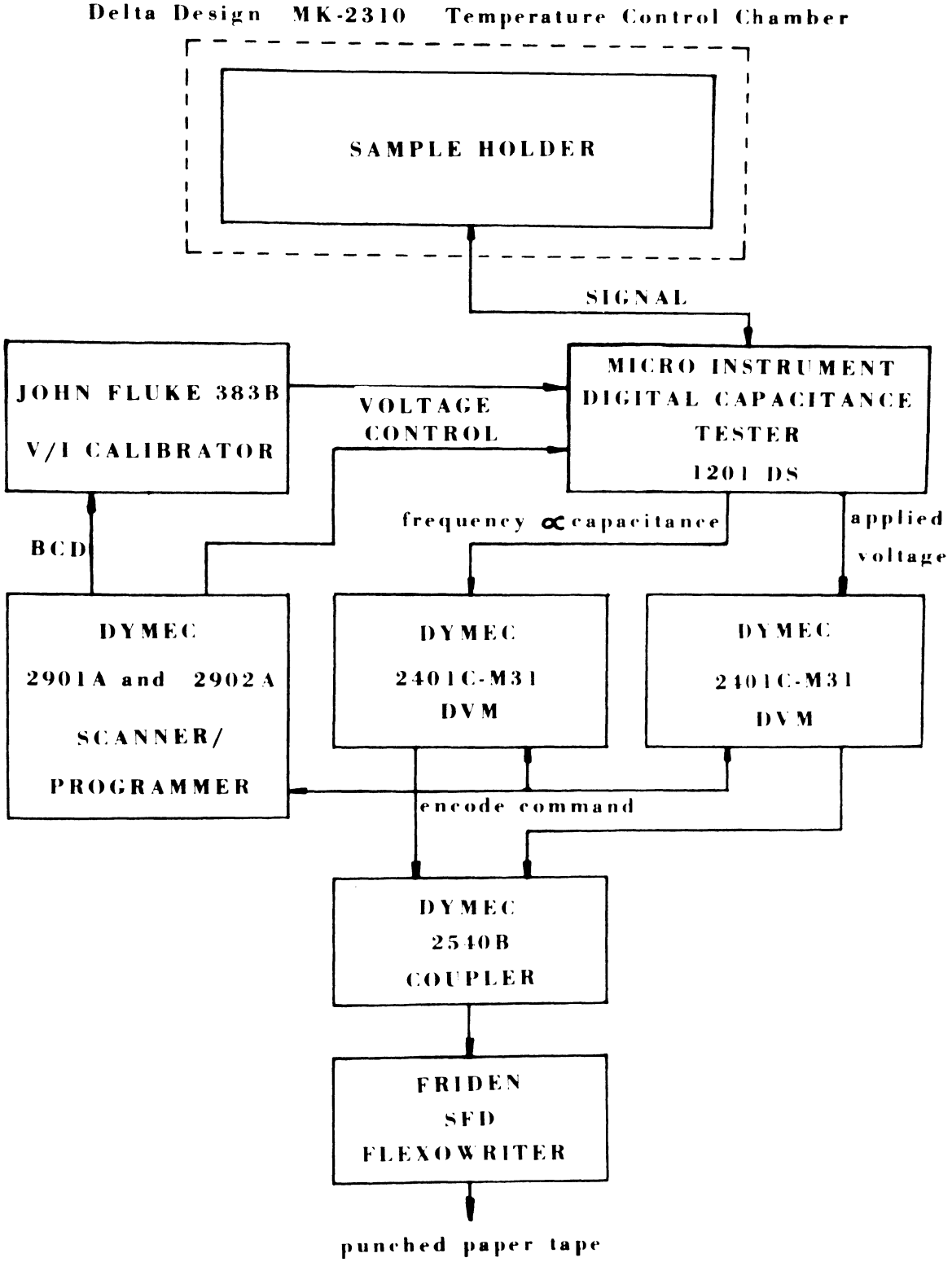

Figure B-2. Capacitance-voltage system block diagram.

REFERENCES

B1. C. A. Goben, "Nuclear Radiation Effects on Silicon p-n Junctions," Technical Progress Report, Document COO-1624-24, Space Sciences Research Center, University of Missouri - Rolla, 1970.

APPENDIX C: MINORITY CARRIER LIFETIME MEASUREMENT

1. Reverse Recovery Characteristics of Diodes

When a diode is switched from conduction in a forward bias to a reverse bias condition, instead of a high impedance immediately appearing across the diode, a momentary low impedance, which is indicated by a very low voltage across the diode, immediately occurs after the switching. This is due to the storage of minority carriers in the semiconductor material.

As the junction is suddenly reverse biased the excess minority carriers must either be swept out of the junction or recombine with excess majority carriers before a high reverse impedance can be obtained.

A typical display of diode reverse recovery characteristics is shown in Figure C-1. In Figure C-1, there are three areas of particular interest.

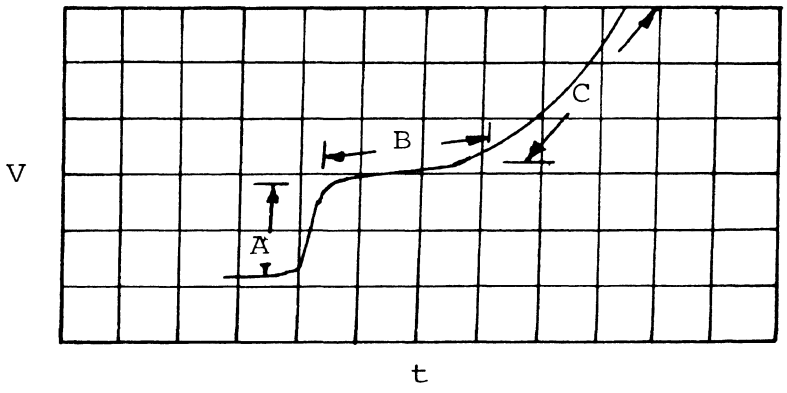

Figure C-1. Typical display of diode reverse recovery characteristics.

These areas are designated by A, B and C. The sudden voltage drop at area A

occurs at the time when forward conduction ceases. During forward conduction, this voltage drop is produced by the internal series resistance across the diode[C1]. When forward current is cut off, this voltage drop disappears, producing the voltage step. Immediately after the sudden drop at area A the voltage decays exponentially for a relatively long period of time (area B). During this interval, minority carriers in the semiconductor material are being swept out by the reverse current. The length of time required for the reverse current to remove the minority carriers gives an indication of the amount of charge stored in the material. The stored charge is found to be proportional to the forward current passing through the junction just before the diode is switched off. If zero reverse current is drawn from the diode, the voltage decay is due entirely to the recombination of minority carriers. By measuring the rate at which the voltage across the diode decays for this case, the effective lifetime can be found.

When the minority carriers in the semiconductor material have either been swept out or have recombined, the depletion region increases at the junction due to the movement of the majority carriers away from the junction. Further reverse current is then required to charge the capacitance of this depletion region (area C). This accounts for the rise in voltage across the junction. The junction capacitance is also dependent on the voltage. The capacitance does not remain constant, but varies with the voltage across the junction.

2. The Effective Lifetime of Minority Carriers

During the period of forward current conduction, excess minority carriers are injected into the semiconductor material. These excess minority

carriers are in addition to the fixed number of minority carriers present resulting from thermal generation of electron-hole pairs. The effective lifetime of these excess minority carriers is the time required for the number of the minority carriers to decrease to 36.7% (1/e) of the original number after termination of the forward current. The effective lifetime expresses the relative rate at which the minority carriers recombine and is a constant for a given diode at a particular absolute temperature and biasing scheme. In general, it does not depend on either the forward or the reverse current drawn from the diode unless neutron induced defects are present. Effective lifetimes should be specified with the temperature at which the measurements were made.

When the measured time (t) is small compared to the effective lifetimes and where kT/q is much smaller than the voltage across the diode, the approximation for the effective lifetime shown below holds[C1]:

$$\tau \simeq \frac{kT}{q} \cdot \frac{\Delta t}{\Delta V} \qquad \text{(C-1)}$$

At room temperature, equation (C-1) becomes

$$\tau\,(300^{o}K) \simeq \frac{0.026}{(\Delta V/\Delta t)} \qquad \text{(C-2)}$$

In equation (C-1), it is assumed that t is small compared to τ. This means that the decay rate of the voltage across the junction should be measured just after the forward current is switched off. Mathematically stated, $\Delta V/\Delta t$ should be measured as $t \rightarrow t_o$, where t_o is the time when the forward current is switched off. The assumption that kT/q is much smaller than the voltage across

the diode also holds quite generally as $t \to t_o$. Therefore, equation (C-2) should be rewritten as:

$$\tau \ (300^{o}K) \simeq \frac{0.026}{(\Delta V/\Delta t)} \Big|_{t \to t_o} \qquad \text{(C-3)}$$

Figure C-2 shows a typical waveform used to measure the effective lifetime of minority carriers. The Tektronix Oscilloscope Type 555[C2] with the Tektronix Type S Recovery-time plug-in Unit[C3] is used for the measurements.

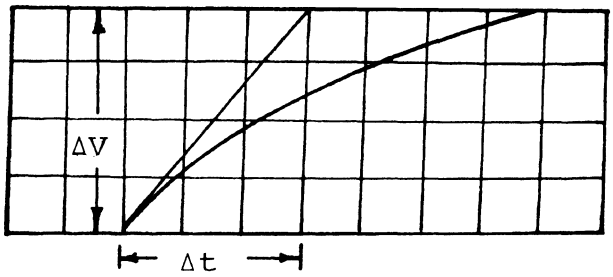

Figure C-2. Tangent line for calculating the voltage decay rate across the diode.

The wave forms used to measure the effective minority carrier lifetime were photographed by a Tektronix Type 100 camera with a Polariod back. Figure C-3 shows two typical pictures which are used to illustrate the decrease in minority carrier lifetimes.

3. Minority Carrier Lifetimes in the Space-Charge and Bulk Regions of a Junction Transistor

For measuring the lifetimes of a transistor, both the emitter-base and collector-base junctions are treated as diodes. Using the method described

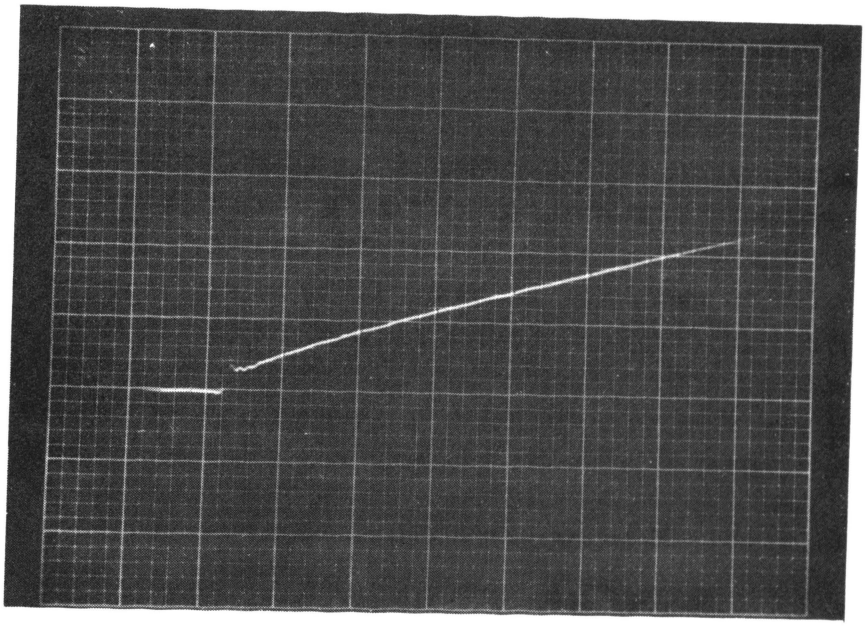

$\Phi = 0$

$$\tau \simeq \frac{0.026}{\frac{(0.05).(0.6)}{(0.1).(1.6)}}$$

$\simeq 139.2$ ns

(at 300°K)

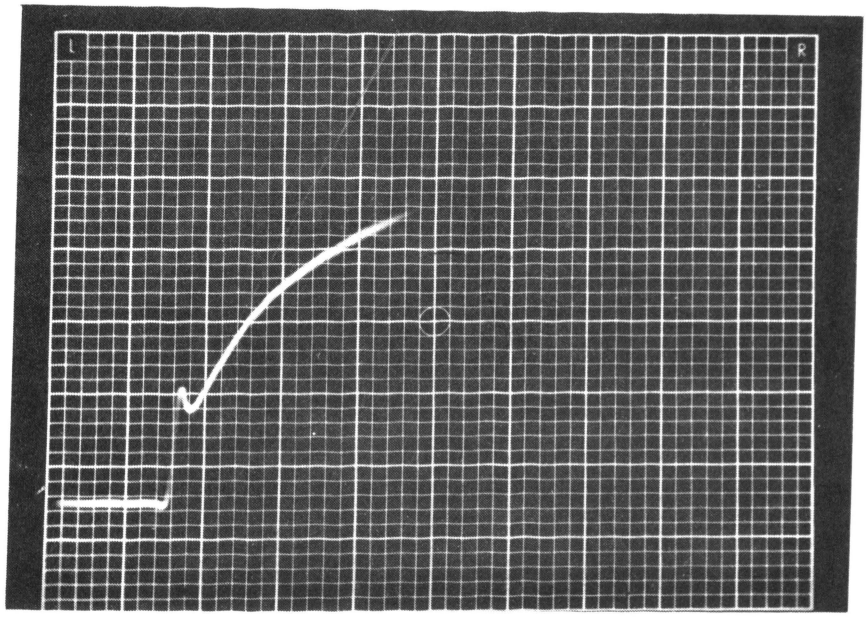

$\Phi = 3 \times 10^{13}$ nvt

$$\tau \simeq \frac{0.026}{\frac{(0.05).(0.4)}{(0.1).(0.2)}}$$

$\simeq 26$ ns

(at 300°K)

Figure C-3. Photographs from which measurements of τ_{BE} at two different fluences are made.

above, the values of τ_{BE} and τ_{BC} for the emitter-base and collector-base junction lifetimes respectively are calculated. The minority carrier lifetimes in the base and collector regions are τ_B and τ_C, respectively, and are related to τ_{BE} and τ_{BC} according to:

$$1/\tau_B + 1/\tau_C = 1/\tau_{BC}, \tag{C-4}$$

and,

$$1/\tau_B \simeq 1/\tau_{BE}, \tag{C-5}$$

or,

$$\tau_B \simeq \tau_{BE}, \tag{C-6}$$

$$\tau_C \simeq (\tau_{BE} - \tau_{BC}) / \tau_{BC} \cdot \tau_{BE}. \tag{C-7}$$

Some difficulty was experienced in fitting the tangent line to the waveforms of low lifetime devices (heavily gold doped or highly irradiated transistors) because of the presence of considerable noise immediately after forward conduction was switched off. This was resolved by assuming that the complete waveform could be accurately described by a simple exponential function. The exponential function was fitted from data in the noise free regions and then the zero point tangent computed.

REFERENCES

C1. S. K. Lederhandler and L. J. Giacoletto, "Measurement of Minority Carrier Lifetime and Surface Effects in Junction Devices," Proc. IRE, 43: 477-483, 1955.

C2. "Tektronix Type 555 Oscilloscope Manual," Tektronix Inc., Beaverton, Oregon, 1964.

C3. "Tektronix Type S Plug-in Unit Manual," Tektronix Inc., Beaverton, Oregon, 1960.

APPENDIX D: NUCLEAR REACTOR FACILITY AND DOSIMETRY

1. Nuclear Reactor Facility

The neutron irradiations for this investigation were performed at the Research Reactor of the University of Missouri - Rolla. This reactor is used both for laboratory training and research by the faculty and students of the University of Missouri - Rolla and other nearby universities. A table of the major reactor characteristics of the Research Reactor of the University of Missouri - Rolla is illustrated in Figure D-1.

The Research Reactor of the University of Missouri - Rolla is a "swimming pool" type reactor, installed in a windowless, concrete, brick and steel structure. The pool consists of a thick walled pit, 19 feet long, 9 feet wide and 27 feet deep, containing 32,000 gallons of pure water. The reactor core is suspended near the bottom of the pool and is covered with some 19 feet of shielding water. The water is continuously purified by an ion exchanger, which removes cations and anions, preventing corrosion and contamination.

The reactor grid plate, containing several rows of fuel pin holes and 22 fuel elements, is a racklike aluminum tray. Open positions in the grid plate are available as sample holders in experiments. Position B2, (see Figure D-2) which is mapped for fast flux irradiations, was used in this investigation. The maximum fast flux ($E > 0.01$MeV) available at 10 kW for position B2 is 8.48×10^{10} neutrons/cm^2-sec. The gamma to fast neutron ratio is approximately 1.1×10^{-8} rad (Si)/$n \cdot cm^{-2}$. D1

Type	Swimming pool type (modified BSR-type), housed in a windowless, concrete, brick and steel structure.
Core	Heterogeneous 90% U-235 enriched uranium oxide-Aluminum-water.
Moderator	Light water.
Reflector	Light water.
Coolant	Light water.
Biological shield	Light water and normal concrete.
Critical mass	Approximately 2.7 kilograms of U-235.
Power level	Up to 200 kw.
Maximum thermal flux	1.5×10^{12} neutrons/cm^2-sec.
Maximum fast flux (E > 10 keV)	2.25×10^{11} neutrons/cm^2-sec.
Fuel elements	MTR type; each fuel element has 10 fuel plates, each plate approximately 17 gms of U-235. Each fuel element is 3"x 3"x 36". The reactor has 22 full fuel elements: 1 left hand half elements, 2 right hand half elements, and 4 control rod elements(3 shim-safety rod, 1 regulating rod).
Auxiliary equipment	Neutron diffraction multi-channel analyzer, nuclear counting equipment; neutron generator, subcritical assembly, neutron chopper.

Figure D-1. Table of technical data for the UMR Research Reactor.

A1	A2	A3	A4	A5	A6	A7	A8	A9
B1	B2	B3	B4	S	B6	B7	B8	B9
C1	C2	C3	F	F	X	O	C8	C9
D1	D2	F	X	F	F	F	F	D9
E1	E2	F	X	F	X	F	F	E9
F1	F2	PT	F	F	F	PT	F8	F9

F = Fuel
S = Source
O = Sample Rotator
X = Control Rods
PT = Pneumatic Transfer Tubes

Figure D-2. Core configuration 31-T.

A photograph of the sample holder which was used to contain the transistors in all of the irradiations is shown in Figure D-3.

2. Foil Activation Analysis for Neutron Fluence Determination

a) Nickel Foil Activation

Determination of neutron fluence during each irradiation run is important for radiation damage studies and has to be accurately ascertained. The approximate desired fast neutron fluence level can be obtained from previously calibrated time-fluence curves at different reactor power levels of the reactor. However, because of fuel depletion and flux pattern variations in the reactor core with time, it is essential to determine the exact fast neutron fluence for each irradiation.

The fundamental problem in prior fast neutron spectrum measurements is that much of the fast neutron energy spectrum lies below the threshold reactions in materials. Careful attention was focused on relations in the keV and MeV range for this purpose. The desirable criteria for a threshold detector such as nickel are as follows: The effective threshold of the materials must be from 0.1 MeV to 15 MeV and sensitive to fast neutrons only. The product should decay to produce a prominent peak which is easily identified between 0 and 2 Mev. It should be formed in sufficient quantity to allow for reasonable detection statistics. The half life of the product nucleus should be of the order of hours or days. A half life of this order will emit enough radiation for good detection in reasonable activation time. Nickel conforms to the above criteria and is ideal in determining flux in the energy range of interest. Ni^{58} (n,p) Co^{58} is the reaction of interest. This threshold reaction has an effective threshold of 2.9 Mev. The effective activation

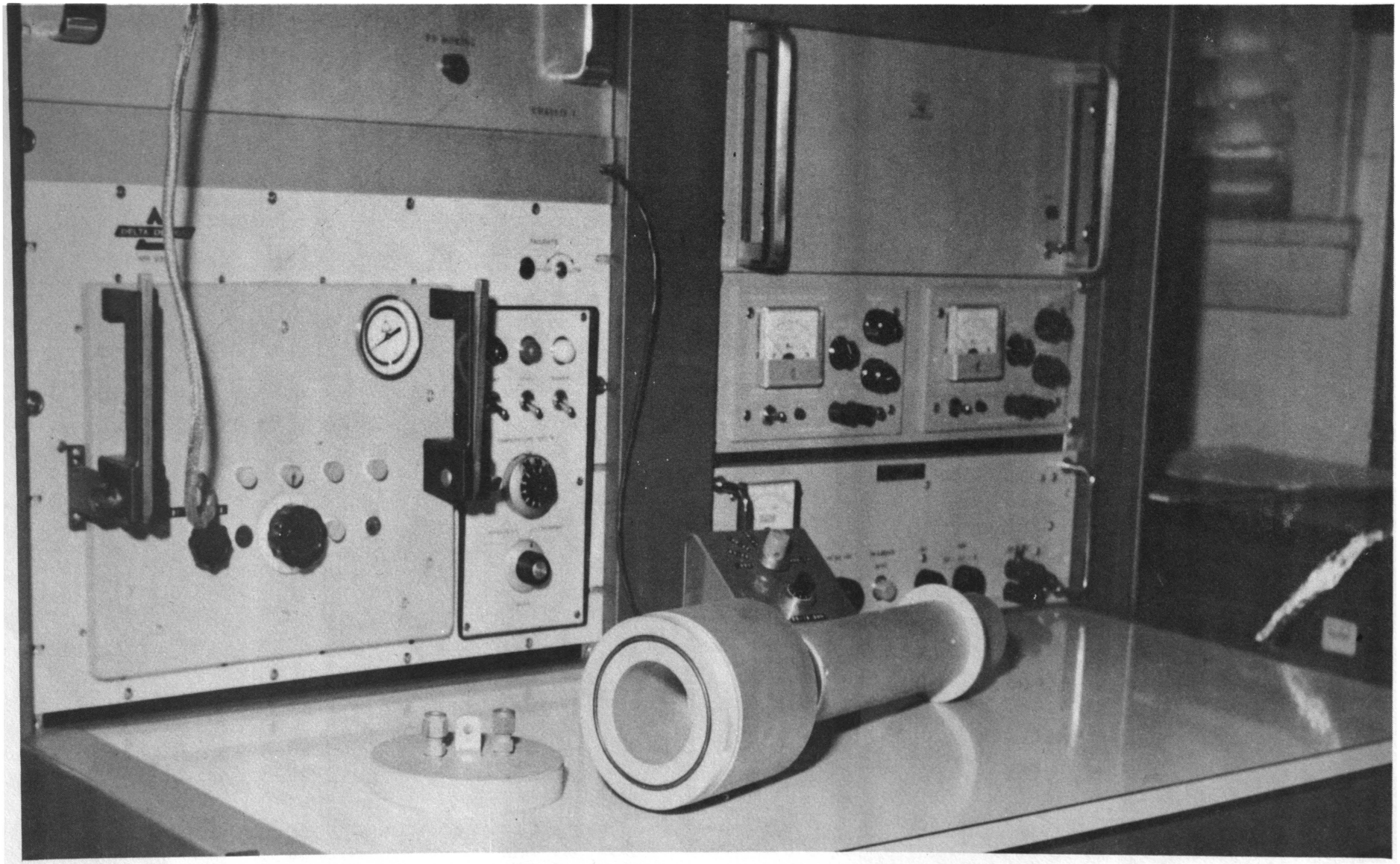

Figure D-3. Photograph of sample holder.

cross-section is 0.42 barns. The daughter, Co^{58}, decays with a half life of 71.3 days. The Ni used in the present investigations is 99.997% pure, obtained from Reactor Expt., Inc.

b) Table of Nuclear Reactions

Reaction	γ Peak (MeV)	Reaction Energy (MeV)	Half Life	Cross Section (millibarns)
Ni^{58} (n,p) Co^{58}	0.81	2.9	72d	92
Ni^{58} (n,p) Co^{58n}	0.81	4.1	9.2h	10
Ni^{58} (n, 2n) Ni^{57}	1.37, 1,87	11.7	36h	0.0012
Ni^{60} (n,p) Co^{60}	1.17, 1.33	2.07	5.24y	3.5
Ni^{61} (n,p) Co^{61}	0.068	5.41	1.65h	-
Ni^{62} (n,α) Fe^{59}	1.13, 1.28	0.884	45.1d	0.014
Ni^{62} (n,p) Co^{62}	1.17, 1.47	8.92	13.9m	-

c) Spectrum Analysis

The Co^{58} obtained from Ni^{58} (n,p) reaction may be detected free from interference by other reactions produced by neutrons on nickel. This product has a gamma photopeak at 0.81 Mev and threshold reaction at 2.9 Mev. The long half life of Co^{58} (72 days) allows for Ni^{57} and Co^{58} to be eliminated allowing a few half lives of decay. The long half life (5.24 years) plus the low cross section of the Ni^{60} (n,p) reaction eliminates interference from Co^{60}. Co^{58} obtained from Ni^{58} (n,p) reaction may be detected free from interference by all other activities produced by neutrons on nickel. However, interference due to the Co^{60} formed from thermal capture by Co^{58} may be troublesome for long irradiations and large fluxes. It was noted that Co^{58} has a thermal burnout of 1% for

thermal fluxes greater than 10^{15} neutrons/cm^2 -sec. Hogg, Weber and Leats[D2] have shown that the isomeric state of Co^{58} has an extremely large cross section of 178,000 barns and therefore must be guarded against and corrected for[D3]. However, the UMR reactor has a thermal flux around $2.5x10^{12}$, and this phenomenon need not be emphasized. Furthermore, the Ni foils were Cd covered as a precaution.

d) Counting Technique

The nickel foils used are one-half inch in diameter and approximately 0.003" thick, weighing about 0.086 gms. After irradiation, the foils are allowed to cool for about 30 hours, in order to allow the decay of short-lived isotopes, so that they will not interfere with the 0.81 Mev peak obtained for the 71.3 day half life of Co^{58}. The foil-induced activity was determined by counting the gamma emission with dual right angle cylindrical 3"x3" sodium iodide thallium activated crystals in conjunction with a 400 channel analyzer. The crystals are adjusted so that they could be closed tightly on the foil to give a 4 π counting geometry. The crystals are located in a lead shield counting chamber in the reactor bay. The multi-channel analyzer is calibrated quantitatively, using known standards Cs-137, Rd-226 and Co-60. The phctopeaks from the foil are then located by channel. The above settings are counted for 1/16 setting corresponding to 0 - 4 MeV range. The calibration chart is shown in Fig. D-4. The background counts for each channel are taken and subtracted from the observed counts for each channel. [Note: The background count is known to change with the reactor operating at different power levels.] The total counts vs. channel

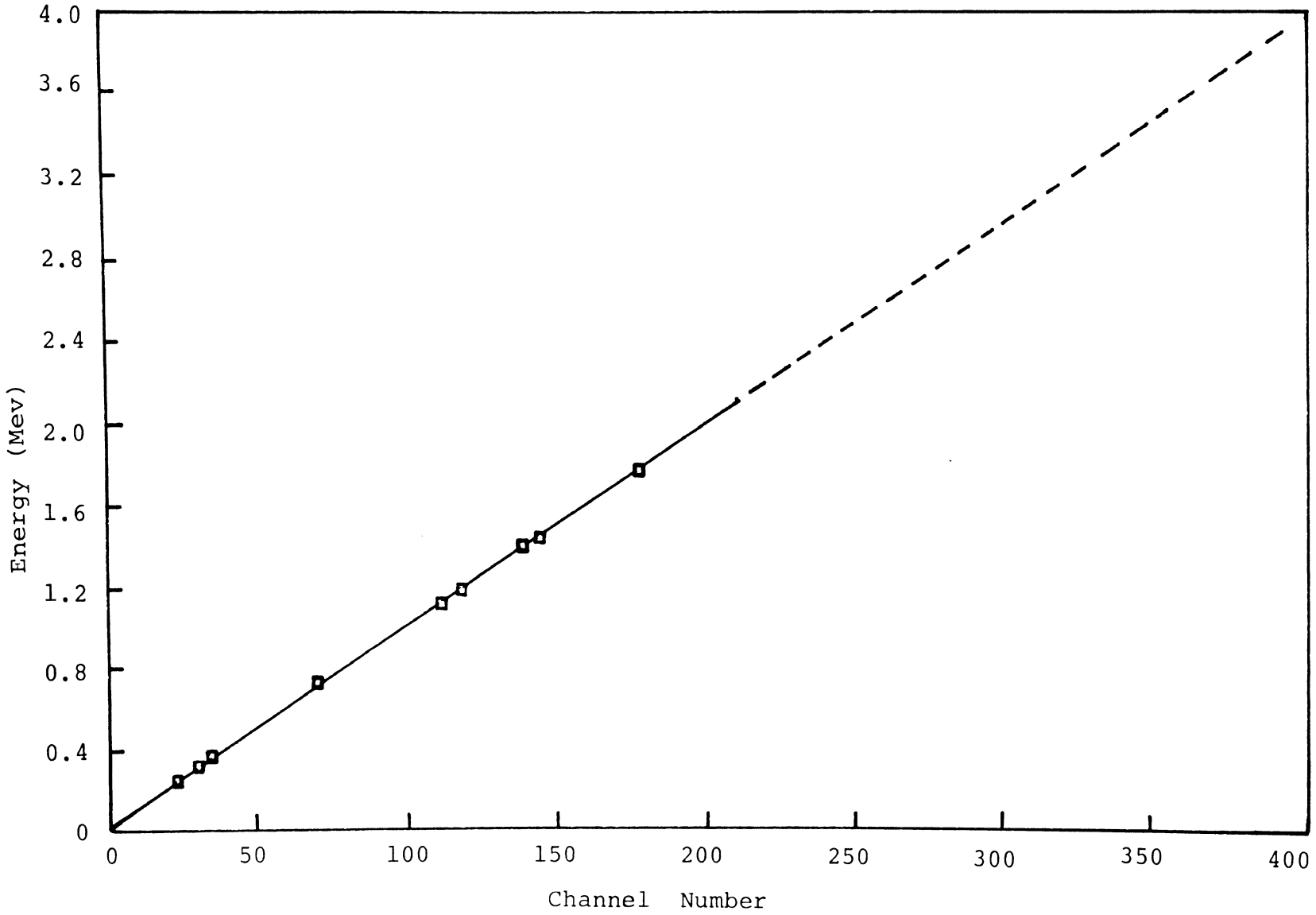

Figure D-4. Calibration Spectra for the Multichannel Analyzer.

number for a certain counting period are plotted. The area under the 0.81 Mev photopeak is then determined. The empirical relation for the fluence (n/cm^2) for energies >10keV can then be directly given by the formula[D4]:

$$\Phi = \frac{1.325 \times 10^{10} \times A}{Wt \times T_3 (1 - \lambda T_2)}$$

where, Φ = neutron fluence (time-integrated flux), in neutrons/cm^2

A = area under 0.81 Mev peak, corrected after subtracting background

Wt = weight of foils being irradiated, gms

T_2 = time to count (cooling time), hrs

T_3 = counting time, minutes

λ = decay constant for $Co^{58} = 4.07 \times 10^{-4}\ hr^{-1}$

The 0.81 Mev peak occurs on channel #81 in the 0 - 4 Mev range.

e) RIDL Model 34-12B Transistorized 400-Channel Analyzer

The RIDL Model 10-8 Scintillation Probe is a convenient detector-preamplifier combination assembly built into a cylindrical container. The housing includes a crystal holder at one end, a photomultiplier tube at the center, and a built-in two-transistor preamplifier at the opposite end.

A 1.75" sodium iodide thallium-activated crystal was used with the scintillation probe.

3. Irradiation Problems

The transistors used in this neutron radiation effects study were irradiated in a double-walled aluminum sample holder having the inner space filled with boron

carbide. The boron carbide shield is needed to allow only fast neutrons (E > 10 keV) to bombard the devices. Boron carbide has a high capture cross section for slow neutrons.

The aluminum used in the fabrication of the sample holder contained impurities whose radioactive half life was long compared with aluminum. As a result, the sample holder could not be removed from the pool until this radioactive decay decreased to a point which was considered safe by the reactor personnel. A cadmium cylinder was used to shield the sample holder from the thermal neutrons causing this activation. This allowed the samples to be removed from the pool on the day they were irradiated. At higher reactor power levels, the temperature inside the sample chamber would tend to increase, requiring a flow of nitrogen through the sample chamber during irradiation to cool the devices. This coolant was necessary to insure that annealing did not take place during irradiation.

REFERENCES

D1. T. A. Niemeier, "Inversion Layer Growths by Gamma Irradiation," Unpublished Research, University of Missouri - Rolla, Rolla, Missouri, 1969.

D2. C. H. Hogg, D. L. Weber and E. C. Leats, Transactions of American Nuclear Society, 4, 271, 1962.

D3. T. O. Parsell and R. L. Heath, "Cross Section of Threshold Detectors for Fission Neutrons; Nickel as a Fast Flux Monitor," Nuclear Science, E: 10, 308-315, 1961.

D4. D. R. Edwards, Unpublished Research, University of Missouri - Rolla, Rolla, Missouri.

APPENDIX E: COBALT 60 IRRADIATION FACILITY AND DOSIMETRY

1. Cobalt-60 Facility

The Cobalt-60 gamma facility, at the University of Missouri Columbia is housed below grade level in a 16-foot deep pool of demineralized water. The source is comprised of ten stainless steel clad cylinders of Cobalt each measuring 11.52 inches long and 0.44 inches in diameter. The capsules are equally spaced around the circumference of a right circular cylinder having an inner diameter of 5.53 inches. The support cylinder has an outside diameter of 7.5 inches and a height of 12.3 inches. The original source strength was 5650 curies on November 12, 1965 and delivered an in-air gamma dose of 6,563 (± 5%) rads/ min. at 1 meter. Fig. E-1 gives the exponential decay patterns for the source. The curie strength and the dose rate in rads/hour at 1 Meter (in air) are plotted versus the time in years.

The source may be utilized for irradiations in air or in water. The facility is equipped with a chain-drive elevator system that moves the source from the pool into the gamma irradiation room with a transit time of 1 minute and 39 seconds. The control panel for the elevator system is located on the wall outside the irradiation room maze. A safety interlock on the elevator system allows entrance to the room only when the source is at the bottom of the pool. Entrance at any other time will disengage a mechanical clutch and the source will drop to the bottom of the pool. A flashing "in-air" warning light, located in the maze corridor, gives visual indication when the source is not fully at the bottom of the pool.

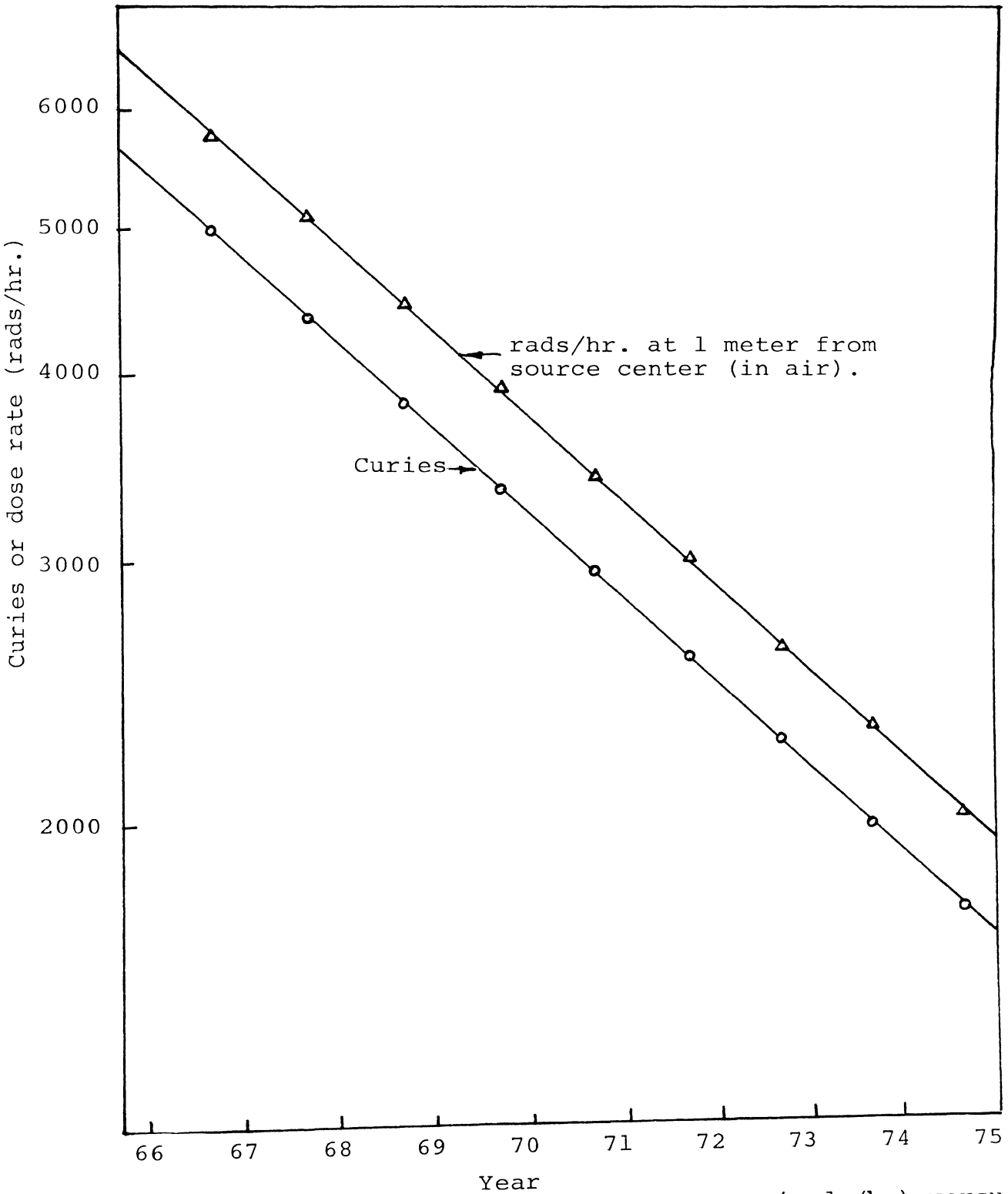

Figure E-1. Curie strength and dose rate (rads/hr) versus time (years) for Co-60 source.

2. Dosimetry

Gamma dose rate measurements are made by ferrous ammonium sulfate (Fricke) or with thermal luminescent dosimeters. In the present investigation both in-air and in-water gamma dose rate measurements were made using the Fricke dosimetric method described below.

The chemical reaction which is the most widely used for Fricke dosimetry is the oxidation of ferrous ions to ferric ions in 0.8 normal solution of sulphuric acid. This system[E1] has been found to be satisfactory over a wide range of conditions. The method most satisfactory for preparing the solutions is[E2]: dissolved 2 g of $FeSO_4 \cdot 7H_2O$ or $Fe(NH_3)_2(SO_4)_2 \cdot 6H_2O$, 0.3 g NaCl and 110 cm^3 concentrated (95-98%) H_2SO_4 (analytical reagent grade) in sufficient distilled water to make 5 liters of solution. (The chloride ions inhibit the oxidation of ferrous ions by certain organic impurities in the system.)

The aliquots are filled with Fricke solution and placed in the sample chamber, together with the devices being irradiated. The exact time period for each irradiation run is noted, for both in-air and in-water irradiations.

The common method for determining the amount of ferric ion which has been produced by the absorbed radiation is spectrophotometric analysis. The ferric ion absorption has a maximum at approximately 304μh. To determine the amount of Fe^{+++}, the transmission of the irradiated sample is compared with that of a non-irradiated sample. A Beckman model DB spectrophotometer equipped with a thermostated hydrogen lamp and quartz cell is used.

The dose rate is given by the formula[E2]:

$$R(\text{rads/hr}) = \frac{10^9}{\epsilon b Y t} \quad (A_{sample} - A_{blank})$$

$$= \frac{2.83 \times 10^4 \, (A_{sample} - A_{blank})}{bt}$$

where

A_{sample} and A_{blank} = absorbancy (optical density of irradiated and unirradiated solutions respectively).

ϵ = molar extinction coefficient

Y = ferrous sulfate yield in micromoles of ferric ions/liter per 1000 rads.

b = sample cell thickness, in cm.

t = irradiation time in hrs.

The ferrous sulfate dosimetric method is suitable for measuring doses in the range of 10^3 to 4.0×10^4 rads, and hence cannot be used for larger absorbed doses. The indications of the dosimeter are independent of the radiation energy within 0.03 Mev - 30 MeV and for dose rates up to about 10^8 rads/sec[E3]. Since total dose values in the present investigation exceed the maximum measurable by Fricke dosimetry, calibration is necessary, assuming a linear relationship between absorbed dose and time.

REFERENCES

E1. W. J. Price, Nuclear Radiation Detection, Second Edition, pp. 295-297, McGraw-Hill Book Company, New York, 1966.

E2. J. A. Weiss, A. O. Allen, and H. A. Schwarz, "Proceedings of the International Conference of the Peaceful Uses of Atomic Energy," Vol. 14, p. 179, United Nations, New York, 1956.

E3. I. V. Vereshchinskii and A. K. Pikaev, "Introduction to Radiation Chemistry," Academy of Sciences of the U. S. S. R., Institute of Physical Chemistry, p. 291-295, 1964.

APPENDIX F: BULK AND SURFACE DAMAGE EFFECTS AS RELATED TO THE PROBLEM OF NUCLEAR RADIATION OF SEMICONDUCTOR DEVICES

Much work has been done on both permanent and transient radiation effects on semiconductor materials and semiconductor devices[F1,F2]. A very small amount of work has involved detailed examination of the degradation of transistor current gain[F3-F7]. Most of the investigations have centered on characterizing parameters at particular bias conditions[F8-F17], or in measuring the effects of radiation on bulk semiconductor materials.

Transient radiation effects in semiconductor materials and devices are associated with the creation, by ionization, of excess hole-electron pairs. Transient radiation effects disappear after the exciting radiation is removed in times on the order of the minority carrier lifetime. Permanent radiation effects are associated with damage to the lattice, whether or not the damage anneals out with time and temperature. Sander[F17] has recently shown that significant annealing is completed in times of the order of tens of seconds after the irradiation is stopped. Hood[F18] found the remaining damage to be stable at room temperature with less than a three percent change in 3,000 hours, although recent studies[F19] indicate a somewhat larger change. The permanent damage with which this research is concerned is the room temperature stable permanent damage.

Surface effects in silicon transistors have been considered to be unpredictable because the response of a semiconductor p-n junction to ionizing radiation varies with initial surface conditions and junction bias during irradiation. Ionizing

radiation induced surface effects in silicon bipolar transistors have been studied by several investigators[F20-F29], using electrons, Co-60 gamma rays and X-rays as radiation sources. The degradation in silicon surface properties is manifested by the depletion or inversion of surfaces[F25, F26], changes in surface recombination velocity and p-n junction characteristics[F27, F28]. Certain radiation environments, such as those found in the core of a swimming pool reactor, have a combined neutron and gamma field which will simultaneously induce surface and bulk damage in semiconductor devices. A typical swimming pool reactor has a gamma dose of 1.8×10^4 rads (Si) which accompanies a neutron fluence of 1.6×10^{12} neutrons/cm^2 ($E > 10$eV). Hence, at lower values of neutron fluence, where the gamma dose is appreciable, surface effects caused by ionizing radiation, dominate the changes in transistor characteristics. But surface effects generally saturate at about 10^6 rads (this corresponds to a neutron flux of approximately 10^{14} neutrons/cm^2). In the study of bulk damage constant, minority carrier lifetime, etc, the contribution due to the surface effects should be taken into consideration. In contrast to bulk effects, the surface radiation effects are very poorly understood and in general not characterized very well. Several years ago, before the present sophistication in surface processing, experiments were carried out in an attempt to characterize radiation surface effects (changes in junction current, breakdown voltage, current gain, etc.) No systematic picture evolved, although surface cleanliness seemed certain to play some role. Transistors that have been made after refinements in junction formation and surface treatment techniques have in the last few years been examined in a variety of gamma-ray environments[F20-F26].

Crystal lattice defects caused by radiation damage act as recombination sites and hence decrease the minority carrier lifetime. Crystal lattice defects, through impurity scattering and compensation of shallow impurities, reduce the carrier mobilities and the carrier concentration. Fast neutron irradiation is particularly damaging to crystal lattices because thousands of atoms may be removed from their lattice sites as the result of a single collision[F29].

The observed decrease in transistor current gain resulting from exposure of transistors to neutron irradiation had, in the past, been attributed primarily to the neutron-induced reduction in minority carrier lifetime in the base region, that is, to the resultant reduction of the base recombination term[F3-F7]. Recent investigations[F30, F31] have shown that the fall off of the transistor current gain at low currents in non-irradiated transistors is caused by the reduction in the emitter efficiency. This suggested that emitter efficiency was important in transistor gain changes resulting from irradiation. To ascertain the role of emitter efficiency, a more detailed study of the degradation of transistors in a radiation environment was required. Such a study was reported by Goben and Smits[F32] in 1964.

Several components of base current have been identified in non-irradiated transistors. The first of these, the bulk recombination-generation current, or the ideal diffusion current for uniform base situation by Moll and Ross[F34]. It has a voltage dependence of exp (qV/kT). The second component is a recombination current in the transition (space-charge) region. The voltage dependence of this second component approximates exp (qV/2kT) at low current densities[F35].

A third component, the surface-perimeter component, has been found to originate at the perimeter of the emitter[F30, F31, F36], that is, where the emitter-base junction intersects the surface. Iwersen et al.[F30] suppressed this component by placing a guard ring on the emitter and applying a bias from emitter contact to guard ring. The voltage dependence of this particular component of current varies as exp (qV/nkT), where n is approximately 1.5. A fourth component, the surface current, stems from surface channels and varies with voltage as exp (qV/mkT), where m is usually between two and four for silicon junctions, although values larger than four have been noted for large channels[F30, F35, F36].

As was shown in the work by Goben and Smits[F28], neutron radiation of p-n junction devices produces a component of current which varies as exp (qV/nkT), where n is approximately 1.5 at room temperature and varies from 1.3 to 1.7 as the temperature ranges from 100°C to -50°C. This component of current is induced in the bulk transition region and dominates the transistor current gain over a wide range of current levels. These findings imply that emitter efficiency played a much more important role in radiation-induced changes in current gain than had been assumed in the past.

In 1964, Goben[F28, F37] reported a base current with a voltage dependence of exp (qV/nkT), n = 1.5, which was observed to increase in proportion to neutron fluence upon exposure to neutron radiation. From a study of the base resistance through which this current component flows, Goben[F28, F37] showed that this component is of bulk and not of perimeter origin and must be attributed to recombination in the bulk space-charge region. This current component dominates transistor

gain over a wide range of current density and is primarily responsible for degradation of transistor current gain by decreasing the emitter efficiency. Goben[F38] (1965) in the analyses of the deviation of the characteristics from an exponential caused by the emission concentration in "ring dot" structures and the transverse bias dependence of the base current components for a special "tetrode-type" test structure, found that the small "1.5 component" of current initially present is indeed of surface-perimeter origin while the added "1.5 component" of current induced by neutron bombardment is of bulk space charge origin. As investigation was made of many different types of silicon transistors, and all were found to exhibit a similar neutron induced component. In this work, Goben[F38] also found an apparent difference in annealing rates for the neutral base region and the space-charge region of the emitter-base junction.

Work by Goben et al.[F39] (1968) indicated, from a study of base and collector current as a function of the emitter-to-base voltage, that the neutron-induced base current has components originating in the emitter space-charge region as well as the neutral base region. At low injection levels the neutron-induced base current was dominated by the space-charge component, whereas the high injection behavior appeared to be controlled by recombination in the neutral base region. Additional experiments performed in special tetrode transistors and van der Pauwtype samples indicated that changes in collector current were dominated by recombination in the neutral base, while changes in base doping and mobility had only a secondary effect. These conclusions were reached from experiments on transistors with a ring emitter, on tetrode type test transistors, and on special Hall effect devices.

Chott and Goben[F40] (1967) found indications that the origin of the anomalous annealing was one, or a combination, of the following mechanisms: a quasi-tunneling recombination phenomena in the emitter-base space-charge region, or a dependence of the neutron-induced defect centers on the p-n junction field. A field dependence appeared to be present, but it was not certain whether the quasi-tunneling phenomena occurred, although it was shown that it is possible for such phenomena to occur. The annealing characteristics of the defects causing changes in the collector and base currents were obtained. Three sets of devices were irradiated and then annealed, with one set having a forward bias during annealing, one set having no bias, and one set having a reverse bias. The dependence of the field on annealing was present but appeared quite complex. The presence of the externally applied field during annealing appeared to enhance the annealing of neutron-induced defects regardless of whether the junction was forward or reverse biased. Su et al.[41] (1968) have shown that the neutron-induced defect clusters in silicon transistors behave differently in the high field emitter-base "space-charge" region than in the low field "neutral" bulk-base region both during introduction and annealing. This anomalous behavior in both formation and annealing has been attributed by some authors to carrier density effects[F42] or to a modification of the defect cluster by the presence of an electric field.[F40, F41]

Recent investigations of neutron-induced defect structures in bulk semiconductors have led to the postulation of a spherical low-density region of disorder surrounded by a space-charge region. Gossick[F43] and Cleland and Crawford[F44] visualize this region as being depleted of charge carriers and acting essentially as an insulating void, thereby, limiting local current flow. Cleland

and Crawford[F44] have shown both theoretically and experimentally that voids in the matrix will indeed change the bulk conductivity and Hall coefficient of semiconductor materials. Other methods for corroborating the existence of the Gossick cluster model, inculding low angle x-ray diffraction and annealing studies, have been carried out by Stein[F45], Whan[F46], and Fujita and Gonser[F47]. Attempts by Parsons et al.[F48] to view the cluster with an electron microscope met with limited success in that the defect regions could be recognized, but their geometries were in question. Bertolotti[F49] has been able to photograph replicas of the defect regions with surprising clarity. He was able to show that the neutron-induced defects in his experimental samples were indeed spherical with regions of altered structure as predicted by Gossick's model[F43]. Very graphic evidence that a space charge region does exist around the disordered regions has been obtained by Bertolotti[F49], using the replica technique. The replicas are observed to contain regions which appear as small hills with a crater at the center. The dimensions of the crater (assumed to be the region of highly localized damage) and the hill (assumed to be the effective radius of the space charge region) correspond exactly to those expected from the disordered region model. The disordered regions are described in the model as being heavily damaged with a defect concentration of $\sim 5 \times 10^{18}$ cm^{-3}, i.e. one lattice site in every 10,000[F43]. The material in the disordered region is therefore considered to be crystalline.

Very recent experimental evidence obtained by Parsons and Hoelke[F50], showed that the structural characteristics of the disordered regions observed in Ge irradiated with fast neutrons or 100 keV oxygen ions were deduced from

their appearance in diffraction contrast and phase contrast electron microscope images to have an amorphous rather than a crystalline structure. Furthermore, each disordered region is surrounded by a non-uniform strain field extending out to $\sim$ 65A^{o} from the disordered region center. Although the neutron induced defect cluster in bulk semiconductor material has been fairly well characterized, the exact nature of the defect cluster in the space-charge region has yet to be studied.

REFERENCES

F1. "The Effect of Nuclear Radiation on Semiconductor Devices," Batelle Memorial Institute, Radiation Effects Information Center (Columbus, Ohio) REIC Report No. 10, April 30, 1960. and Addendum, July 15, 1961.

F2. F. Larin, Radiation Effects in Semiconductor Devices, p. 3, Wiley, New York, 1968.

F3. J. K. Loferski, "Analysis of the Effect of Nuclear Radiation on Transistors," Journal of Applied Physics, 29, 35-40, 1958.

F4. G. C. Messenger and J. P. Spratt, "The Effects of Neutron Irradiation on Germanium and Silicon," Proceedings IRE, 46, 1038-1044, 1958.

F5. J. W. Easley and J. A. Dooley, "On the Neutron Bombardment Reduction of Transistor Current Gain," Journal of Applied Physics. 31, 1024-1028, 1960.

F6. J. A. Hood, "Predicting the Current Gain Degradation in n-p n Silicon Transistors after Irradiation by High-Energy Neutrons," Sandia Laboratory (Albuquerque, N. M.) (Publication) SC-TM-64-69, 1964.

F7. J. W. Easley, "Radiation Damage to Semiconductor Devices," Sandia Laboratory (Albuquerque, N. M.) (Publication) SCR-532,1962.

F8. D. G. DeNure, "Effect of Fast Neutron Bombardment on Type 2N559 and 2N559E Epitaxial p-n-p Germanium Switching Transistors," Bell Telephone Laboratory (Murray Hill, N. J.) (Publication) MM-61-4252-33, 1961.

F9. J. A. Hood, "Degradation of n-p-n Silicon Planar Transistors with Bombardment by High-Energy Neutrons," Sandia Laboratory (Albuquerque, N. M.) (Publication) SC-TM-261-73 (14), 1963.

F10. J. A. Hood, "Neutron Induced Degradation of Commercial Transistors," Sandia Laboratory (Albuquerque, N. M.) (Publication) SC-TM-129 63 (14), 1963.

F11. C. I. Westmark and W. H. Rice "Radiation-Induced Degradation of DC Current Gain and Collector-to-Emitter Saturation Voltage for Selected Power Transistors," Sandia Laboratory (Albuquerque, N. M.) (Publication) SC-TM-223 63 (14), 1963.

F12. H. H. Sanders, "Neutron Permanent Damage Data for the 2N1675 Transistor," Sandia Laboratory (Albuquerque, N. M.) (Publication) SC R-65-550, 1964.

F13. S. K. Manlief, "A Method of Measuring the Minority Carrier Base Transit Time in a Junction Transistor Exposed to a Neutron Environment," Sandia Laboratory (Albuquerque, N. M.) (Publication) SC-TM-314-63 (14), 1963.

F14. G. F. Levy, R. R. Fouse and S. V. Castner, "The Effects of Nuclear Radiation on Some Selected Semiconductor Devices," Proceedings of the Second Conference on Nuclear Radiation Effects on Semiconductor Devices, Materials and Circuits, 76-81, 1959.

F15. J. J. Loferski, "A Brief Resume of Radiation Effects on Semiconductor Materials and Devices," Proceedings of the Second Conference on Nuclear Radiation Effects on Semiconductor Devices, Materials and Circuits, 8-10, 1959.

F16. F. M. Smits, "On the Energy Dependence of Neutron Damage to Silicon Transistors," Sandia Laboratory (Albuquerque, N. M.) (Publication) SC-R-64-196, 1964.

F17. H. H. Sander, "Room Temperature Annealing of Silicon Transistor Parameters Degraded by a Burst of Neutrons," Sandia Laboratory (Albuquerque, N. M.) (Publication) SC-R-64-192, 1964.

F18. J. A. Hood, "Predicting the Current Gain Degradation in n-p-n Silicon Transistors after Irradiation by High-Energy Neutrons," Sandia Laboratory (Albuquerque, N. M.) (Publication) SC-TM-64-69, 1964.

F19. M. Frank and C. D. Taulbee, "Factors Influencing Prediction of Transistor Current Gain in Neutron Radiation," IEEE Transactions on Nuclear Science, NS-14, 6, 127-133, 1967.

F20. D. S. Peck, R. R. Blair, W. L. Brown and F. M. Smits, "Surface Effects of Radiation on Transistors," The Bell System Technical Journal, 42, 95-129, 1963.

F21. E. H. Snow, H. S. Grove and D. J. Fitzgerald, "Effects of Ionizing Radiation on Oxidized Silicon Surfaces and Planar Devices," Proceedings of the IEEE, 55, 7, 1168-1185, 1967.

F22. P. R. Measel and R. R. Brown, "Low Dose Ionization-Induced Failures in Acitve Bipolar Transistors," IEEE Transactions on Nuclear Science, NS-15, 6, 224-231, 1968.

F23. G. J. Brucker, W. J. Dennehy and A. G. Holmes-Siedle, "Ionization and Displacement Damage in Silicon Transistors," IEEE Transactions on Nuclear Science, NS-13, 6, 188-196, 1966.

F24. H. L. Hughes, "Surface Effects of Space Radiation on Silicon Devices," IEEE Transactions on Nuclear Science, NS-12, 6, 53-63, 1965.

F25. W. Poch and A. G. Holmes-Siedle,"A Prediction and Selection System for Radiation Effects in Planar Transistors, "IEEE Transactions on Nuclear Science, NS-15, 6, 213-233, 1968.

F26. M. A. Littlejohn and R. W. Lade, "Influence of Co-60 Gamma Irradiation on the Surface and Bulk Recombination Rates in Silicon," IEEE Transactions on Nuclear Science, NS-14, 6, 305-318, 1967.

F27. D. L. Nelson and R. J. Sweet, "Mechanism of Ionizing Radiation Surface Effects on Transistors," IEEE Transactions on Nuclear Science, NS-13, 6, 197-206, 1966.

F28. R. J. Maier, "Surface Effects on Transistors: Radiation Susceptibility of High Emitter Peripheral Arc Length Devices," USNRDL TR-68-48, 29, March 1968, as cited by R. R. Brown, "Damage of Constants for Surface Effects in Silicon Bipolar Transistors," Presented at IEEE Nuclear and Space Radiation Effects Conference, 1969.

F29. D. S. Billington and J. H. Crawford, Jr., Radiation Damage in Solids, Princeton, N. J., Princeton University Press, pp. 13-36, 1961.

F30. J. W. Iwerson, A. R. Bray and J. J. Kleinmack, "Low-Current Alpha in Silicon Transistors," IRE Transactions on Electron Devices, ED-9, 474-478, 1962.

F31. P. J. Coppen and W. T. Matzen, "Distribution of Recombination Current in Emitter-Base Junctions of Silicon Transistors," IRE Transactions on Electron Devices, ED-9, 75-81, 1962.

F32. C. A. Goben and F. M. Smits, "Anomalous Base Current Component in Neutron Irradiated Transistors," IEEE Radiation Effects Conference, Seattle, Washington, 1964. Also, Sandia Laboratory (Albuquerque, N. M.) (Publication) SC-R-64-194, 1964.

F33. W. Shockley, "The Theory of p-n Junctions in Semiconductors and p-n Junction Devices," Bell System Technical Journal, 38, 435-589, 1949.

F34. J. L. Moll and L. M. Ross,"The Depencence of Transistor Parameters on the Distribution of Base Layer Resistivity," Proceedings IRE, 44, 72-76, 1956.

F35. C. T. Sah, R. N. Noyce and W. Shockley, "Carrier Generation and Recombination in p-n Junctions and p-n Junction Characteristics," Proceedings IRE, 45, 1228-1243, 1957.

F36. C. T. Sah, "Effect of Recombination and Channel on p-n Junction and Transistor Characteristics," IRE Transactions on Electron Devices, ED-9, 94-108, 1962.

F37. C. A. Goben, "Neutron Bombardment Reduction of Transistor Current Gain," Ph.D. Dissertation, Iowa State University Library (Ames, Iowa) 1965. Also, Sandia Laboratory (Albuquerque, N. M.), (Publication) SCR-64-1373, 1964.

F38. C. A. Goben, "A Study of the Neutron-Induced Base Current Component in Silicon Transistors," IEEE Transactions on Nuclear Science, NS-12, 5, 134-146, 1965.

F39. C. A. Goben, F. M. Smits and J. L. Wirth, "Neutron Radiation Damage in Silicon Transistors," IEEE Transactions on Nuclear Science NS-15, 2, 14-29, 1968.

F40. J. R. Chott and C. A. Goben, "Radiation and Annealing Characteristics of Neutron Irradiated Silicon Transistors, "IEEE Transactions on Nuclear Science, NS-14, 6, 134-146, 1967. Also AEC Report COO-1624-4.

F41. L. S. Su, G. E. Gassner and C. A. Goben, " Radiation and Annealing Characteristics on Neutron Bombarded Silicon Transistors," IEEE Transactions on Nuclear Science, NS-15, 6, 95-107, 1968. Also, AEC Report COO-1624-13.

F42. B. L. Gregory and H. H. Sander, "Injection Dependence of Transient Annealing in Neutron-Irradiated Silicon Devices," IEEE Transactions on Nuclear Science, NS-14, 6, 116-126, 1967.

F43. B. R. Gossick, "Disordered Regions in Semiconductors Bombarded by Fast Neutrons," Journal of Applied Physics, 30, 1214-1218, 1959.

F44. J. W. Cleland and J. H. Crawford, Jr., "Nature of Bombardment Damage and Energy Levels in Semiconductors," Journal of Applied Physics, 30, 1204, 1959.

F45. H. J. Stein, "Transitory Electrical Properties of n-Type Germanium," Journal of Applied Physics, 31, 1309-1318, 1960.

F46. R. E. Whan, "Oxygen Defect Complexes in Neutron Irradiated Germanium," Journal of Applied Physics, 37, 3378, 1966.

F47. F. R. Fujita and U. Gonser, "Small Angle Scattering of X-Rays by Deutron-Irradiated Germanium Crystal," Journal of Physical Society of Japan, 13, 1068-1069, 1958.

F48. J. R. Parsons, R. W. Balluffi and J. S. Koehler, "Direct Observation of Neutron Damage in Germanium," Applied Physics Letters, 13, 57-58, 1962.

F49. M. Bertolotti, "Experimental Observation of Damage Clusters in Semiconductors," in Radiation Effects in Semiconductors, edited by F. L. Vook (Plenum Press) New York, pp. 311-330, 1968.

F50. J. R. Parsons and C. W. Hoelke, "Observation of Crystal Lattice Planes in Neutron and Ion Bombarded Ge," IEEE Transactions on Nuclear Science, NS-15, 6, 80-86, 1969.